Vibration Control of Structures with Self-Sensing Piezoelectric Actuators Incorporating Adaptive Mechanisms

LAW Wai Wing

A Thesis Submitted in Partial Fulfillment

of the Requirement for the Degree of

Master of Philosophy

in

Mechanical and Automation Engineering

January 2002

ABSTRACT

The coupling effect of an electric field with a mechanical deformation makes piezoelectric materials feasible for sensing or actuating functions in structural applications. Recently, a self-sensing actuator for controlling a structure is proposed. It uses a single piece of piezoelectric element to serve as both sensor and actuator simultaneously. This technique achieves truly sensor-actuator collocation and reduces the weight of the structural system. However, the self-sensing configuration inherently contains a feed forward dynamics. In order to achieve self-sensing actuation, the feed forward signal due to control input must be separated so that the sensing signal is resulting from the mechanical response only. The feed forward dynamics is related to the equivalent capacitance of the piezoelectric material and subjected to change in the ambience. In addition, due to the relatively high amplitudes of the control signal to the mechanical response, sensing signal can be corrupted with a small capacitance variation. For closed loop applications, this corruption would degrade the system performance or lead to instability. In this research, a self-tuning adaptive algorithm is proposed to compensate for the capacitance variation. The adaptive compensation is applied for structural control. A cantilever beam bonded with a single piezoelectric patch is used to demonstrate the effectiveness of self-sensing actuation. The proposed adaptive algorithm is used to separate the mechanical response from the total response. Concurrently, control input is generated based on the compensated sensing signal to actively damp out the vibration of the cantilever beam. The usefulness of the proposed technique is demonstrated by suppressing the vibration of the structure in both simulations and experimental studies.

摘要

壓電材料的機電偶合特性使它既可以用作感知元件，也可用作驅動元件。最近提出了一種自感知主動控制技術，在這種控制中，壓電材料既做傳感器，也做驅動器，真正實現了傳感和驅動的共存 (collocation)，並且還減輕了結構的重量。然而，自感知技術具有自身固有的前饋特性 (feed forward)，爲了實現自感知驅動，由控制輸入而引起的前饋信號必須被分離出來，以辨識感知信號只是來自機械響應。而前饋特性與壓電材料片的等效電容有關，並隨周邊環境而改變。另外，在機械響應中產生的信號對比起控制輸入有較小的相對幅值。因此，微細的電容變化往往可使感知信號失真。在閉環控制中，這種損耗可影響控制的整體表現，並或導致失穩。在本文的研究中，提出了一種自調節 (self-tuning) 技術，用以補償壓電片電容的改變。這種自調節補償技術將應用于結構控制中。當中一個貼上壓電片的懸臂梁將用來顯示自感知驅動技術于振動控制中之效能。本文提出的自調節技術將用來從整個響應信號中，將機械響應的部分分離出來。同時，控制輸入也是基于這補償後的感知信號而產生。最終，本文提出的技術將通過模擬和實驗來驗證其主動控制結構振動之有效性。

ACKNOWLEDGEMENTS

I would like to express my sincere gratitude to my supervisor Prof. Huang Jie and co-supervisor Prof. Liao Wei Hsin for their patient instruction and guidance throughout my research study. I would also like to thank my committee members, Prof Yam Yeung and Prof. Li Wen Jung, for their constructive suggestions on this research.

I further wish to thank my close colleagues at Applied Control and Computing Laboratory, including Dr. D. Wang, Dr. J. Wang, K. Yeung, W.Y. Lan, Y.C. Liu and Z.Y. Chen for their encouragement and friendship. Thanks are also delivered to Neil Ching and Eric Wong for their valuable experiment experiences and supports.

Finally, appreciation is also expressed to all my family members for their thoughtful care and concerns for me.

CONTENTS

LIST OF FIGURES

LIST OF TABLES

Chapter 1

Introduction

1.1 Background

1.1.1 Piezoelectric Materials

Piezoelectricity was firstly discovered by Curie brothers in 1880. They formulated the coupling effect between electric field and mechanical deformation. This electromechanical coupling property has been leading to numerous sensing or actuating applications. From direct piezoelectric effect, signal is induced due to material deformation. Since piezoelectric material has the advantage of high strain sensitivity, it can measure strain as low as 10^{-8}, and makes piezoelectric material suitable to be used as a sensor with high resolution. On the other hand, because of the converse piezoelectric effect, piezoelectric material can be deformed by an electric field in a controlled manner. In addition, its quick response time, high efficiency and large force authority also make the piezoelectric materials feasible in various actuating applications.

The major limitation of piezoelectric ceramics is their brittle nature. Also, piezoelectric material exhibits certain degree of hystersis nonlinearity with large applied field. In any case, piezoelectric material cannot be used in measuring DC signal and thus limits its usage in AC applications.

The fast growing field of smart materials and structures is experiencing demands for high precision transduction devices. In recent years, the piezoelectric materials have been used extensively as active control elements. Because the piezoelectric materials

can be directly bonded to or embedded into a structure, it has been applied in the field of aerospace, micro-positioning, structural monitoring, optics and computer engineering. It has been shown that the performance is significant and there exists less effect on the original dynamics of the coupled structure.

1.1.2 Self-sensing Actuation

The technique of self-sensing actuation was originated in 1960s and it was proposed to control the electro-magnetic mechanisms of an ordinary speaker. Recently the concept of using a piezoelectric element as a self-sensing actuator has attracted much interest due to the advantages of collocation and system component reduction. Traditionally piezoelectric materials have been used extensively as sensors or actuators to perform a single transducer function. Because of the dual functions of piezoelectric materials that relate electric charge to mechanical stress and mechanical strain to electric field, a piezoelectric element can be used concurrently as a sensor and actuator. The self-sensing configuration achieves perfect sensor-actuator collocation. When comparing with a structure using separated sensor-actuator pairs, self-sensing actuation can reduce the mass added to the overall structure and this can increase the control efficiency with less mass and space.

1.2 Literature Review

Since early 1990, piezoelectric materials have been increasingly used as sensors and actuators. The technique of using a single piece of piezoelectric element as both sensor and actuator concurrently in a closed loop system was firstly proposed by Dosch et al. [5]. They applied collocated control to suppress vibration of a smart structure and experimentally verified the effectiveness of their proposed self-sensing actuation (SSA). Anderson and Hagood [1] applied the SSA technique to a truss structure in which an active piezoelectric strut functioned as a transducer and experimental results showed the strain measurement through SSA agreed closely to that using the conventional strut with an attached strain gauge. Jones and Garcia [12, 9] demonstrated the use of SSA technique to control a piezoelectric-actuated micropositioner and verified the step response performance. Main et al. [16] developed a charge driven control instead of the conventional voltage driven control to study the hysteresis effect and demonstrated that the charge feedback design indeed reduces the hysteresis effect even under the application of a high control gain. Because the self-sensing actuation configuration inherently contains a feedforward dynamics, the success of SSA relies on the compensation of this feed through dynamics such that only the signal induced from the structural deformation is used for generating the control input. As the feedforward dynamics depends on the equivalent capacitance of the piezoelectric material, which is sensitive to varying ambience, Tani et al. [23] demonstrated that the variation of the equivalent piezoelectric capacitance has critical effects on SSA-based closed loop systems. Yang and Jeng [26] demonstrated that the use of SSA would destabilize the closed loop system when it is failed to compensate the feed forward dynamics.

In order to take the variation of the piezoelectric capacitance into account, Takigami et al. [22] used μ synthesis approach to design a robust controller and applied it to suppress the vibration of a cantilever beam. The closed loop performance showed the designed controller has good robustness and performance with respect to the capacitance variation. Vipperman and Clark [24] presented an adaptive compensation technique to deal with the piezoelectric capacitance variation and applied collocated feedback control to suppress structural vibration. The capabilities of both vibration suppression and compensation of capacitance variation had been experimentally verified. Clark et al. [4] extended the above work by using adaptive filtering to compensate the feed through dynamics in an open loop configuration. Pourboghrat and his associates [19, 20] also designed a similar controller incorporating adaptive compensation technique and experimentally verified their design by showing the step responses and vibration suppression capabilities.

1.3 Motivation

In a closed loop self-sensing configuration, the electrical feedforward dynamics associated with the piezoelectric capacitance and control input have to be separated so that the control is generated based on the structural deformation. In the previous researches, it was achieved by using a static design. Because of the ambience dependence of the piezoelectric capacitance, the static design is shown to be insufficient. Although some adaptation techniques have been proposed to deal with the capacitance uncertainty, the vibration controller is only applicable for low frequencies (<100Hz) [24] or the adaptation is designed for open loop structural monitoring, i.e. no concurrent control action is applied [4]. In this thesis, we will develop an adaptive compensation technique to separate the feedforward dynamics and concurrently control the structural vibration such that the modified design could be applied for broad frequency band and simultaneously suppress higher vibration modes even with the variation of piezoelectric capacitance.

1.4 Thesis Organization

In this thesis the problems of modeling, control and implementations of the designed controller to a smart structure are studied. The rest of the thesis is organized as follows:

- Chapter 2 presents the modeling of a smart beam structure using Hamilton's principle. Galerkin's method is applied to discretize the equation of motion to standard state space representation. External sensing circuit is integrated to the beam structure to yield an electromechanical system.
- Chapter 3 presents two types of vibration controller: strain rate feedback and positive position feedback control. An adaptive compensation is proposed and combined with the strain sensing circuit to deal with the PZT capacitance variation. The combined design is investigated by simulations.
- Chapter 4 presents the hardware implementation of the designed controller to the smart beam structure via a digital signal processor. Several experiments are conducted to test the combined adaptive compensation for closed loop systems under different conditions.
- Chapter 5 draws the conclusion of this thesis. Several problems for future work are also suggested.

Chapter 2

Structural Modeling and Formulation

A dynamic model of a smart structure composed of a cantilever beam and a piezoelectric patch will be derived in this chapter. The derived model will be integrated with an external circuit in which sensing and actuation can be functioned simultaneously. The overall electromechanical model will be validated through experiment.

2.1 Overview of Piezoelectricity

The direct piezoelectric effect is the production of a potential difference across the material when it is stressed. Conversely, the material strains upon an application of an electric field. The constitutive equations derived from linear theory of piezoelectricity are as follows [4]:

$$D_i = d_{ikl} T_{kl} + \varepsilon_{ik}^T E_k \tag{2.1}$$

$$S_{ij} = s_{ijkl}^E T_{kl} + d_{kij} E_k \tag{2.2}$$

where D is electric charge, S is strain, T is stress, E is electric field, s is elastic compliance, ε is permittivity and d is piezoelectric constant. The superscripts E and T denote the conditions of constant electric field and constant stress, respectively. The subscripts i, j, k and l take the values of 1, 2 or 3 to specify the direction.

Equation (2.1) states that the total electric charge is proportional to both the stress and applied electric field, which is known as the direct piezoelectric effect. The converse piezoelectric effect is stated in (2.2) that the total strain is proportional to both the applied stress and applied electric field.

For isotropic piezoelectric materials, the constitutive equations are reduced to:

$$D_i = d_{il} T_l + \varepsilon_{ik}^T E_k \tag{2.3}$$

$$S_j = s_{jl}^E T_l + d_{kj} E_k \tag{2.4}$$

2.2 Modeling of the Beam Structure

In this study, we consider a structure composed of a cantilever beam and a single piece of piezoelectric element as shown in Figure 2.1. The dynamics equation of the structural transverse vibration (Z-direction) will be derived. As the structure vibrates, the piezoelectric element will be stressed or compressed longitudinally (X-direction). Owning to the piezoelectricity, signal will be induced across the piezoelectric element. Concurrently, external electric field (Z-direction) is applied to control the structure. From (2.3) and (2.4), the constitutive equations for this beam structure are:

$$D_3 = d_{31} T_1 + \varepsilon_{33}^T E_3 \tag{2.5}$$

$$S_1 = s_{11}^E T_1 + d_{31} E_3 \tag{2.6}$$

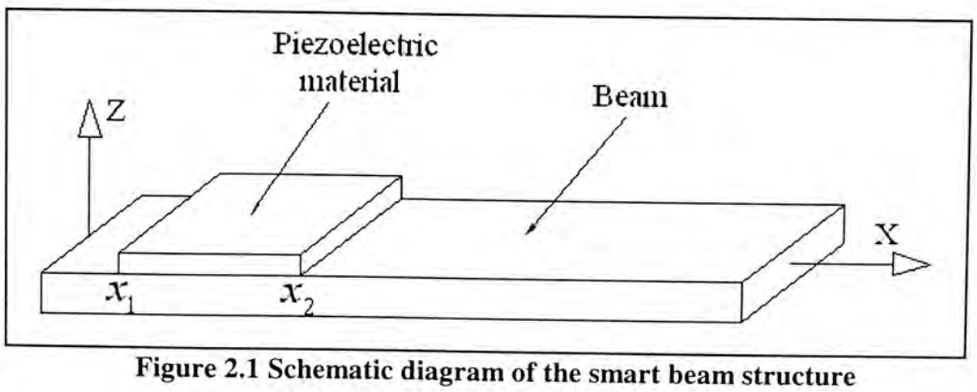

Figure 2.1 Schematic diagram of the smart beam structure

2.2.1 Electromechanical Conversion

From the constitutive equation (2.6), the strain induced by an applied electric field E_3 is $d_{31} E_3$.

The induced force F_1 (in X direction) due to the applied voltage V_a is:

$$F_1 = E_p b_p d_{31} t_p \left(\frac{V_a}{t_p} \right) = E_p b_p d_{31} V_a$$

where E_p , b_p and t_p are the Young's modulus, width and thickness of the piezoelectric element respectively.

The virtual work due to this applied voltage is

$$\delta W_p = F_1 \delta u_p$$

where δu_p is the virtual displacement of the mid plan of the piezoelectric element in the u direction as shown in Figure 2.2.

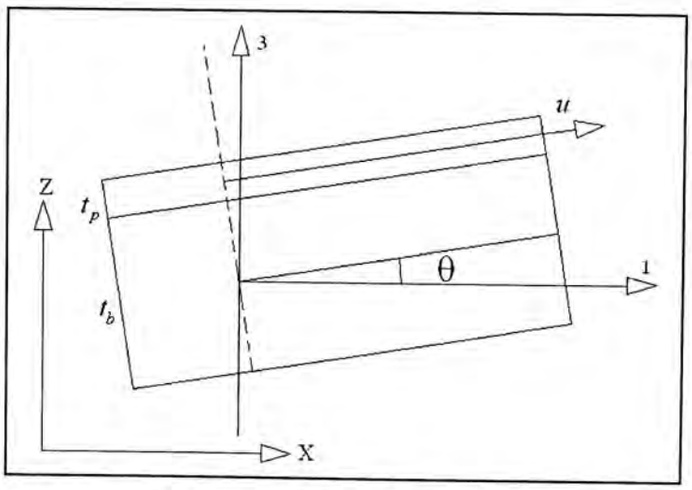

Figure 2.2 An infinitesimal element of the composite beam

Let the transverse displacement of the beam be $w(x,t)$.

Since $\delta u_p = \delta \left(\frac{\partial u_p}{\partial x} \right) dx$ and $u_p = -\left(\frac{t_b + t_p}{2} \right) \frac{\partial w}{\partial x} = -a \frac{\partial w}{\partial x}$

where t_b is the thickness of the beam, $a = \frac{t_b + t_p}{2}$ and $\theta = \frac{\partial w}{\partial x}$

The virtual work due to the applied voltage V_a can be expressed as:

$$\delta W_p = F_1 \delta u = -\int_{x_1}^{x_2} E_p d_{31} a b_p V_a \delta\left(\frac{\partial^2 w}{\partial x^2}\right) dx$$

$$= -\int_0^L E_p d_{31} a b_p V_a \delta\left(\frac{\partial^2 w}{\partial x^2}\right)[H(x-x_1) - H(x-x_2)]dx \qquad (2.7)$$

where x_1 and x_2 are the locations of the piezoelectric element bonded on the beam, L is the length of the beam and H is the Heaviside-step function defined as:

$$H(x-x_1) = \begin{cases} 0 & if \quad x < x_1 \\ 1 & if \quad x \geq x_1 \end{cases} \qquad (2.8)$$

2.2.2 Model Derivation Using Hamilton's Principle

Let $f_d(x,t)$ be the disturbance of the structure. The virtual work due to disturbance is:

$$\delta W_d = \int_0^L f_d(x,t)\delta w(x,t)dx \qquad (2.9)$$

Since the external applied voltage V_a and the disturbance f_d are the only non-conservative forces of the structure, total virtual work due to non-conservative forces is:

$$\delta W_{NC} = \delta W_p + \delta W_d \qquad (2.10)$$

The potential energy of the beam and the piezoelectric element are respectively:

$$V_b = \frac{1}{2}\int_0^L E_b I_b \left(\frac{\partial^2 w}{\partial x^2}\right)^2 dx$$

$$V_p = \frac{1}{2}\int_0^L E_p I_p \left(\frac{\partial^2 w}{\partial x^2}\right)^2 [H(x-x_1) - H(x-x_2)]dx$$

where E is Young's modulus and I is area moment of inertia. The subscripts b and p denote the corresponding values of beam and piezoelectric element.

For simplicity, let $\overline{H}(x, x_1, x_2) = H(x - x_1) - H(x - x_2)$.

So, $$V_p = \frac{1}{2}\int_0^L E_p I_p \left(\frac{\partial^2 w}{\partial x^2}\right)^2 \overline{H}(x, x_1, x_2)dx$$

The kinetic energy of the beam and the piezoelectric element are respectively:

$$T_b = \frac{1}{2}\int_0^L \rho_b A_b \left(\frac{\partial w}{\partial t}\right)^2 dx$$

$$T_p = \frac{1}{2}\int_0^L \rho_p A_p \left(\frac{\partial w}{\partial t}\right)^2 \overline{H}(x, x_1, x_2)dx$$

where ρ is density and A is cross sectional area.

The Lagrangian of the composite structure is the difference of the total kinetic energy to the total potential energy, i.e.

$$L = (T_b + T_p) - (V_b + V_p) \tag{2.11}$$

From (2.10) and (2.11), using extended Hamilton's principle yields:

$$\int_{t_1}^{t_2} (\delta L + \delta W_{NC})dt = 0 \tag{2.12}$$

$$\delta w(x, t_1) = \delta w(x, t_2) = 0 \tag{2.13}$$

Substituting the potential and kinetic energies into (2.12) yields:

$$\int_{t_1}^{t_2} \delta L dt$$

$$= \int_{t_1}^{t_2} \delta(T_b + T_p - V_b - V_p)dt$$

$$= \int_{t_1}^{t_2} \delta\left\{\frac{1}{2}\int_0^L \rho_b A_b \left(\frac{\partial w}{\partial t}\right)^2 dx\right\}dt + \int_{t_1}^{t_2} \delta\left\{\frac{1}{2}\int_0^L \rho_p A_p \left(\frac{\partial w}{\partial t}\right)^2 \overline{H}(x, x_1, x_2)dx\right\}dt$$

$$- \int_{t_1}^{t_2} \delta\left\{\frac{1}{2}\int_0^L E_b I_b \left(\frac{\partial^2 w}{\partial x^2}\right)^2 dx\right\}dt - \int_{t_1}^{t_2} \delta\left\{\frac{1}{2}\int_0^L E_p I_p \left(\frac{\partial^2 w}{\partial x^2}\right)^2 \overline{H}(x, x_1, x_2)dx\right\}dt$$

$$= \int_{t_1}^{t_2}\int_0^L \rho_b A_b\left(\frac{\partial w}{\partial t}\right)\delta\left(\frac{\partial w}{\partial t}\right)dxdt + \int_{t_1}^{t_2}\int_0^L \rho_p A_p\left(\frac{\partial w}{\partial t}\right)\delta\left(\frac{\partial w}{\partial t}\right)\overline{H}(x,x_1,x_2)dxdt$$

$$- \int_{t_1}^{t_2}\int_0^L E_b I_b\left(\frac{\partial^2 w}{\partial x^2}\right)\delta\left(\frac{\partial^2 w}{\partial x^2}\right)dxdt - \int_{t_1}^{t_2}\int_0^L E_p I_p\left(\frac{\partial^2 w}{\partial x^2}\right)\delta\left(\frac{\partial^2 w}{\partial x^2}\right)\overline{H}(x,x_1,x_2)dxdt \quad (2.14)$$

Using integration by parts with respect to t,

$$\int_{t_1}^{t_2}\int_0^L \rho_p A_p\left(\frac{\partial w}{\partial t}\right)\delta\left(\frac{\partial w}{\partial t}\right)\overline{H}(x,x_1,x_2)dxdt$$

$$= \int_0^L \rho_p A_p\left(\frac{\partial w}{\partial t}\right)\overline{H}(x,x_1,x_2)\delta w\Big|_{t_1}^{t_2} dx - \int_{t_1}^{t_2}\int_0^L \rho_p A_p\left(\frac{\partial^2 w}{\partial t^2}\right)\overline{H}(x,x_1,x_2)\delta w dxdt$$

From (2.13): $\delta w(x,t_1) = \delta w(x,t_2) = 0$. Hence,

$$\int_{t_1}^{t_2}\int_0^L \rho_p A_p\left(\frac{\partial w}{\partial t}\right)\delta\left(\frac{\partial w}{\partial t}\right)\overline{H}(x,x_1,x_2)dxdt$$

$$= -\int_{t_1}^{t_2}\int_0^L \rho_p A_p\left(\frac{\partial^2 w}{\partial t^2}\right)\overline{H}(x,x_1,x_2)\delta w dxdt \quad (2.15)$$

Substituting $\overline{H}(x,x_1,x_2) = 1$ and replacing the subscript p in (2.15) by b for the beam:

$$\int_{t_1}^{t_2}\int_0^L \rho_b A_b\left(\frac{\partial w}{\partial t}\right)\delta\left(\frac{\partial w}{\partial t}\right)dxdt = -\int_{t_1}^{t_2}\int_0^L \rho_p A_p\left(\frac{\partial^2 w}{\partial t^2}\right)\delta w dxdt \quad (2.16)$$

Using integration by parts with respect to x

$$- \int_{t_1}^{t_2}\int_0^L E_p I_p\left(\frac{\partial^2 w}{\partial x^2}\right)\delta\left(\frac{\partial^2 w}{\partial x^2}\right)\overline{H}(x,x_1,x_2)dxdt$$

$$= -\int_{t_1}^{t_2} E_p I_p\left(\frac{\partial^2 w}{\partial x^2}\right)\overline{H}(x,x_1,x_2)\delta\left(\frac{\partial w}{\partial x}\right)\Big|_0^L dt + \int_{t_1}^{t_2}\int_0^L E_p I_p\left(\frac{\partial^3 w}{\partial x^3}\right)\delta\left(\frac{\partial w}{\partial x}\right)\overline{H}(x,x_1,x_2)dxdt$$

$$+ \int_{t_1}^{t_2}\int_0^L E_p I_p\left(\frac{\partial^2 w}{\partial x^2}\right)\delta\left(\frac{\partial w}{\partial x}\right)\overline{H}'(x,x_1,x_2)dxdt$$

where $\overline{H}'(x,x_1,x_2) = \dfrac{d}{dx}[H(x-x_1) - H(x-x_2)]$

Since $$\overline{H}(0,x_1,x_2)=\overline{H}(L,x_1,x_2)=0 \tag{2.17}$$

$$-\int_{t_1}^{t_2}\int_0^L E_pI_p\left(\frac{\partial^2 w}{\partial x^2}\right)\delta\left(\frac{\partial^2 w}{\partial x^2}\right)\overline{H}(x,x_1,x_2)dxdt$$

$$=\int_{t_1}^{t_2}\int_0^L E_pI_p\left(\frac{\partial^3 w}{\partial x^3}\right)\delta\left(\frac{\partial w}{\partial x}\right)\overline{H}(x,x_1,x_2)dxdt$$

$$+\int_{t_1}^{t_2}\int_0^L E_pI_p\left(\frac{\partial^2 w}{\partial x^2}\right)\delta\left(\frac{\partial w}{\partial x}\right)\overline{H}'(x,x_1,x_2)dxdt \tag{2.18}$$

Using integration by parts with respect to x again, (2.18) becomes:

$$-\int_{t_1}^{t_2}\int_0^L E_pI_p\left(\frac{\partial^2 w}{\partial x^2}\right)\delta\left(\frac{\partial^2 w}{\partial x^2}\right)\overline{H}(x,x_1,x_2)dxdt$$

$$=\int_{t_1}^{t_2}E_pI_p\left(\frac{\partial^3 w}{\partial x^3}\right)\overline{H}(x,x_1,x_2)\delta w\Big|_0^L dt-\int_{t_1}^{t_2}\int_0^L E_pI_p\left(\frac{\partial^4 w}{\partial x^4}\right)\overline{H}(x,x_1,x_2)\delta w dxdt$$

$$-\int_{t_1}^{t_2}\int_0^L E_pI_p\left(\frac{\partial^3 w}{\partial x^3}\right)\overline{H}'(x,x_1,x_2)\delta w dxdt+\int_{t_1}^{t_2}E_pI_p\left(\frac{\partial^2 w}{\partial x^2}\right)\overline{H}'(x,x_1,x_2)\delta w\Big|_0^L dt$$

$$-\int_{t_1}^{t_2}\int_0^L E_pI_p\left(\frac{\partial^3 w}{\partial x^3}\right)\overline{H}'(x,x_1,x_2)\delta w dxdt-\int_{t_1}^{t_2}\int_0^L E_pI_p\left(\frac{\partial^2 w}{\partial x^2}\right)\overline{H}''(x,x_1,x_2)\delta w dxdt$$

By (2.17) and using the fact $\overline{H}'(0,x_1,x_2)=\overline{H}'(L,x_1,x_2)=0$ (2.19)

$$-\int_{t_1}^{t_2}\int_0^L E_pI_p\left(\frac{\partial^2 w}{\partial x^2}\right)\delta\left(\frac{\partial^2 w}{\partial x^2}\right)\overline{H}(x,x_1,x_2)dxdt$$

$$=-\int_{t_1}^{t_2}\int_0^L E_pI_p\left(\frac{\partial^4 w}{\partial x^4}\right)\overline{H}(x,x_1,x_2)\delta w dxdt-\int_{t_1}^{t_2}\int_0^L E_pI_p\left(\frac{\partial^2 w}{\partial x^2}\right)\overline{H}''(x,x_1,x_2)\delta w dxdt$$

$$-2\int_{t_1}^{t_2}\int_0^L E_pI_p\left(\frac{\partial^3 w}{\partial x^3}\right)\overline{H}'(x,x_1,x_2)\delta w dxdt \tag{2.20}$$

Similarly,

$$\int_{t_1}^{t_2}\delta W_p dt=-\int_{t_1}^{t_2}\int_0^L E_p d_{31}ab_pV_a\delta\left(\frac{\partial^2 w}{\partial x^2}\right)\overline{H}(x,x_1,x_2)dxdt$$

$$= -\int_{t_1}^{t_2}\int_0^L E_p d_{31} a b_p V_a \overline{H}''(x,x_1,x_2)\delta w dx dt \tag{2.21}$$

Hence, the virtual work due to total non-conservative forces is:

$$\int_{t_1}^{t_2} \delta W_{NC} dt = \int_{t_1}^{t_2} \left(\delta W_p + \delta W_d\right) dt$$

$$= \int_{t_1}^{t_2}\int_0^L \left\{f_d(x,t) - E_p d_{31} a b_p V_a \overline{H}''(x,x_1,x_2)\right\}\delta w dx dt \tag{2.22}$$

Using integration by parts twice with respect to x,

$$-\int_{t_1}^{t_2}\int_0^L E_b I_b \left(\frac{\partial^2 w}{\partial x^2}\right)\delta\left(\frac{\partial^2 w}{\partial x^2}\right) dx dt$$

$$= -\int_{t_1}^{t_2} E_b I_b \left(\frac{\partial^2 w}{\partial x^2}\right)\delta\left(\frac{\partial w}{\partial x}\right)\Bigg|_0^L dt + \int_{t_1}^{t_2} E_b I_b \left(\frac{\partial^3 w}{\partial x^3}\right)\delta w\Bigg|_0^L dt$$

$$-\int_{t_1}^{t_2}\int_0^L E_b I_b \left(\frac{\partial^4 w}{\partial x^4}\right)\delta w dx dt \tag{2.23}$$

Substituting (2.15), (2.16), (2.20), (2.22) and (2.23) into (2.12) yield,

$$-\int_{t_1}^{t_2}\int_0^L \rho_b A_b \left(\frac{\partial^2 w}{\partial t^2}\right)\delta w dx dt - \int_{t_1}^{t_2}\int_0^L \rho_p A_p \left(\frac{\partial^2 w}{\partial t^2}\right)\overline{H}(x,x_1,x_2)\delta w dx dt$$

$$-\int_{t_1}^{t_2} E_b I_b \left(\frac{\partial^2 w}{\partial x^2}\right)\delta\left(\frac{\partial w}{\partial x}\right)\Bigg|_0^L dt + \int_{t_1}^{t_2} E_b I_b \left(\frac{\partial^3 w}{\partial x^3}\right)\delta w\Bigg|_0^L dt - \int_{t_1}^{t_2}\int_0^L E_b I_b \left(\frac{\partial^4 w}{\partial x^4}\right)\delta w dx dt$$

$$-\int_{t_1}^{t_2}\int_0^L E_p I_p \left(\frac{\partial^4 w}{\partial x^4}\right)\overline{H}(x,x_1,x_2)\delta w dx dt - \int_{t_1}^{t_2}\int_0^L E_p I_p \left(\frac{\partial^2 w}{\partial x^2}\right)\overline{H}''(x,x_1,x_2)\delta w dx dt$$

$$-2\int_{t_1}^{t_2}\int_0^L E_p I_p \left(\frac{\partial^3 w}{\partial x^3}\right)\overline{H}'(x,x_1,x_2)\delta w dx dt$$

$$+\int_{t_1}^{t_2}\int_0^L \left\{f_d(x,t) - E_p d_{31} a b_p V_a \overline{H}''(x,x_1,x_2)\right\}\delta w dx dt = 0 \tag{2.24}$$

Since (2.24) holds for arbitrary δw, rearranging (2.24), the equation of motion can be expressed as:

$$E_b I_b\left(\frac{\partial^4 w}{\partial x^4}\right)+\rho_b A_b\left(\frac{\partial^2 w}{\partial t^2}\right)+\left\{E_p I_p\left(\frac{\partial^4 w}{\partial x^4}\right)+\rho_p A_p\left(\frac{\partial^2 w}{\partial t^2}\right)\right\}\overline{H}(x,x_1,x_2)$$

$$+E_p I_p\left(\frac{\partial^2 w}{\partial x^2}\right)\overline{H}''(x,x_1,x_2)+2E_p I_p\left(\frac{\partial^3 w}{\partial x^3}\right)\overline{H}'(x,x_1,x_2)$$

$$=-E_p d_{31} a b_p V_a \overline{H}''(x,x_1,x_2)+f_d(x,t) \tag{2.25}$$

with boundary conditions:

$$\left(\frac{\partial^2 w}{\partial x^2}\right)\delta\left(\frac{\partial w}{\partial x}\right)\Bigg|_0^L=0 \quad \text{and} \quad \left(\frac{\partial^3 w}{\partial x^3}\right)\delta w\Bigg|_0^L=0 \tag{2.26}$$

For a cantilever beam, the boundary conditions are constrained at both ends. At the fixed end, the displacement and slope of the beam are zero. Hence,

$w(0,t)=0$ (zero displacement)

$\frac{\partial w(0,t)}{\partial x}=0$ (zero slope)

At the free end, the bending moment and shear force are zero. Hence,

$\frac{\partial^2 w(L,0)}{\partial x^2}=0$ (zero bending moment)

$\frac{\partial^3 w(L,0)}{\partial x^3}=0$ (zero shear force)

2.3 Discretization of Equation of Motion

In the previous section, the equation of motion of a smart cantilever beam undergoing transverse vibration is derived. Its dynamics is found to be governed by a forth order partial differential equation (PDE). In most cases, PDE systems do not admit closed form solution. Hence, in this section, an approximation technique will be employed to convert the original PDE to ordinary differential equation (ODE) system.

Using Galerkin's discretization technique, the approximate solution of (2.25) takes the form of space-time separable functions:

$$w(x,t) = \sum_{i=1}^{n} \phi_i(x) q_i(t) \tag{2.27}$$

where $q_i(t)$ is a time function, $\phi_i(x)$ is a set of independent trial spatial functions satisfying all boundary conditions and n is the number of modes of interest. In this study, the set of trial function $\phi_i(x)$ is chosen to be the eigenvectors of the plain cantilever beam, i.e.,

$$\phi_i(x) = C_1 \cosh(\beta_i x) + C_2 \sinh(\beta_i x) + C_3 \cos(\beta_i x) + C_4 \sin(\beta_i x) \tag{2.28}$$

with
$$\phi_i(0) = \phi_i^{(1)}(0) = \phi_i^{(2)}(L) = \phi_i^{(3)}(L) = 0 \tag{2.29}$$

where β_i are the solution of:

$$\beta_i L \cosh(\beta_i L) + 1 = 0 \tag{2.30}$$

and (C_1, C_2, C_3, C_4) can be determined from the boundary conditions.

Since the approximate solution (2.27) does not exactly satisfy the partial differential equation (2.25) and incurs some error ε, substituting (2.27) into (2.25) and the incurred error ε is found to be:

$$\begin{aligned}
&E_b I_b \sum_{i=1}^{n} \phi_i^{(4)}(x) q_i(t) + \rho_b A_b \sum_{i=1}^{n} \phi_i(x) \ddot{q}_i(t) \\
&+ \left[E_p I_p \sum_{i=1}^{n} \phi_i^{(4)}(x) q_i(t) + \rho_p A_p \sum_{i=1}^{n} \phi_i(x) \ddot{q}_i(t) \right] \overline{H}(x, x_1, x_2) \\
&+ 2E_p I_p \sum_{i=1}^{n} \phi_i^{(3)}(x) q_i(t) \overline{H}'(x, x_1, x_2) + E_p I_p \sum_{i=1}^{n} \phi_i^{(2)}(x) q_i(t) \overline{H}''(x, x_1, x_2) \\
&+ E_p d_{31} a b_p V_a \overline{H}''(x, x_1, x_2) - f_d(x,t) = \varepsilon
\end{aligned}$$

The error is minimized in the directions defined by the set of eigenvectors. Setting the inner product of the error and each eigenvector to zero yields:

$$\langle \varepsilon \quad \phi_j \rangle = \int_0^L \varepsilon \phi_j dx = 0 \quad for \quad j = 1,2,...,n$$

$$\Rightarrow \left[\rho_b A_b \left(\sum_{i=1}^{n} \int_0^L \phi_i(x)\phi_j(x)dx \right) + \rho_p A_p \left(\sum_{i=1}^{n} \int_0^L \phi_i(x)\phi_j(x)\overline{H}(x,x_1,x_2)dx \right) \right] \ddot{q}_i(t)$$

$$+ \left[E_b I_b \left(\sum_{i=1}^{n} \int_0^L \phi_i^{(4)}(x)\phi_j(x)dx \right) + E_p I_p \left(\sum_{i=1}^{n} \int_0^L \phi_i^{(4)}(x)\phi_j(x)\overline{H}(x,x_1,x_2)dx \right) \right] q_i(t)$$

$$+ \left[2E_p I_p \left(\sum_{i=1}^{n} \int_0^L \phi_i^{(3)}(x)\phi_j(x)\overline{H}'(x,x_1,x_2)dx \right) \right] q_i(t)$$

$$+ \left[E_p I_p \left(\sum_{i=1}^{n} \int_0^L \phi_i^{(2)}(x)\phi_j(x)\overline{H}''(x,x_1,x_2)dx \right) \right] q_i(t)$$

$$+ E_p d_{31} ab_p V_a \left(\int_0^L \overline{H}''(x,x_1,x_2)\phi_j dx \right) - \int_0^L f_d(x,t)\phi_j(x)dx = 0 \qquad (2.31)$$

Using integration by parts twice and (2.29)

$$\int_0^L \phi_i^{(4)}(x)\phi_j(x)dx = \int_0^L \phi_i^{(2)}(x)\phi_j^{(2)}(x)dx \qquad (2.32)$$

Using integration by parts and (2.17),

$$\int_0^L \phi_i^{(3)}(x)\phi_j(x)\overline{H}'(x,x_1,x_2)dx$$

$$= \phi_i^{(3)}(x)\phi_j(x)\overline{H}(x,x_1,x_2)\Big|_0^L - \int_0^L \phi_i^{(4)}(x)\phi_j(x)\overline{H}(x,x_1,x_2)dx$$

$$- \int_0^L \phi_i^{(3)}\phi_j^{(1)}(x)\overline{H}(x,x_1,x_2)dx$$

$$= -\int_0^L \phi_i^{(4)}(x)\phi_j(x)\overline{H}(x,x_1,x_2)dx - \int_0^L \phi_i^{(3)}\phi_j^{(1)}(x)\overline{H}(x,x_1,x_2)dx \qquad (2.33)$$

Similarly, using integration by parts and (2.19),

$$\int_0^L \overline{H}''(x,x_1,x_2)\phi_j(x)dx = \overline{H}'(x,x_1,x_2)\phi_j(x)\Big|_0^L - \int_0^L \overline{H}'(x,x_1,x_2)\phi_j^{(1)}(x)dx$$

$$= -\overline{H}(x,x_1,x_2)\phi_j^{(1)}(x)\Big|_0^L + \int_0^L \overline{H}(x,x_1,x_2)\phi_j^{(2)}(x)dx$$

$$= \int_0^L \overline{H}(x, x_1, x_2)\phi_j^{(2)}(x)dx$$

$$= \phi_j^{(1)}(x_2) - \phi_j^{(1)}(x_1) \tag{2.34}$$

Again, by (2.17), (2.19) and integration by parts,

$$\int_0^L \phi_i^{(2)}(x)\phi_j(x)\overline{H}''(x, x_1, x_2)dx$$

$$= \phi_i^{(2)}(x)\phi_j(x)\overline{H}'(x, x_1, x_2)\Big|_0^L - \int_0^L \phi_i^{(3)}(x)\phi_j(x)\overline{H}'(x, x_1, x_2)dx$$

$$- \int_0^L \phi_i^{(2)}(x)\phi_j^{(1)}(x)\overline{H}'(x, x_1, x_2)dx$$

$$= -\phi_i^{(3)}(x)\phi_j(x)\overline{H}(x, x_1, x_2)\Big|_0^L + \int_0^L \phi_i^{(4)}(x)\phi_j(x)\overline{H}(x, x_1, x_2)dx$$

$$+ \int_0^L \phi_i^{(3)}(x)\phi_j^{(1)}(x)\overline{H}(x, x_1, x_2)dx - \phi_i^{(2)}(x)\phi_j^{(1)}(x)\overline{H}(x, x_1, x_2)\Big|_0^L$$

$$+ \int_0^L \phi_i^{(3)}(x)\phi_j^{(1)}(x)\overline{H}(x, x_1, x_2)dx + \int_0^L \phi_i^{(2)}(x)\phi_j^{(2)}(x)\overline{H}(x, x_1, x_2)dx$$

$$= \int_0^L \left[\phi_i^{(4)}(x)\phi_j(x) + 2\phi_i^{(3)}(x)\phi_j^{(1)}(x) + \phi_i^{(2)}(x)\phi_j^{(2)}(x)\right]\overline{H}(x, x_1, x_2)dx \tag{2.35}$$

Substituting (2.32), (2.33), (2.34) and (2.35) into (2.31), it gives:

$$\left[\rho_b A_b\left(\sum_{i=1}^n \int_0^L \phi_i(x)\phi_j(x)dx\right) + \rho_p A_p\left(\sum_{i=1}^n \int_0^L \phi_i(x)\phi_j(x)\overline{H}(x, x_1, x_2)dx\right)\right]\ddot{q}_i(t)$$

$$+\left[E_b I_b\left(\sum_{i=1}^n \int_0^L \phi_i^{(2)}(x)\phi_j^{(2)}(x)dx\right) + E_p I_p\left(\sum_{i=1}^n \int_0^L \phi_i^{(4)}(x)\phi_j(x)\overline{H}(x, x_1, x_2)dx\right)\right]q_i(t)$$

$$-2E_p I_p\left\{\sum_{i=1}^n \int_0^L \left[\phi_i^{(4)}(x)\phi_j(x) + \phi_i^{(3)}(x)\phi_j^{(1)}(x)\right]\overline{H}(x, x_1, x_2)dx\right\}q_i(t)$$

$$+E_p I_p\left\{\sum_{i=1}^n \int_0^L \left[\phi_i^{(4)}(x)\phi_j(x) + \phi_i^{(2)}(x)\phi_j^{(2)}(x)\right]\overline{H}(x, x_1, x_2)dx\right\}q_i(t)$$

$$+2E_p I_p\left(\sum_{i=1}^n \int_0^L \phi_i^{(3)}(x)\phi_j^{(1)}(x)\overline{H}(x, x_1, x_2)dx\right)q_i(t)$$

$$+E_p d_{31} a b_p V_a\left(\phi_j'(x_2) - \phi_j'(x_1)\right) - \int_0^L f_d(x,t)\phi_j(x)dx = 0$$

$$\Rightarrow \quad \left[\rho_b A_b\left(\sum_{i=1}^{n}\int_0^L \phi_i(x)\phi_j(x)dx\right)+\rho_p A_p\left(\sum_{i=1}^{n}\int_{x_1}^{x_2}\phi_i(x)\phi_j(x)dx\right)\right]\ddot{q}_i(t)$$

$$+\left[E_b I_b\left(\sum_{i=1}^{n}\int_0^L \phi_i^{(2)}(x)\phi_j^{(2)}(x)dx\right)+E_p I_p\left(\sum_{i=1}^{n}\int_{x_1}^{x_2}\phi_i^{(2)}(x)\phi_j^{(2)}(x)dx\right)\right]q_i(t)$$

$$+E_p d_{31} a b_p V_a\left(\phi_j'(x_2)-\phi_j'(x_1)\right)-\int_0^L f_d(x,t)\phi_j(x)dx=0 \qquad (2.36)$$

Here, assume the disturbance is of the form of a discrete force, i.e.,

$$f_d(x,t)=f_d(t)\delta(x-x_d)$$

where $\delta(x-x_d)$ is the Dirac delta function: $\delta(x-x_d)=\begin{cases}\infty & at \quad x=x_d\\ 0 & for \quad x\neq x_d\end{cases}$

Hence, the disturbance term appearing in the equation of motion can be expressed as:

$$\int_0^L f_d(t,x)\phi_j(x)dx=\int_0^L f_d(t)\delta(x-x_d)\phi_j(x)dx$$

$$=f_d(t)\phi_j(x_d) \qquad (2.37)$$

Using the following substitutions:

$$M_{ij}=\rho_b A_b\int_0^L \phi_i(x)\phi_j(x)dx+\rho_p A_p\int_{x_1}^{x_2}\phi_i(x)\phi_j(x)dx \qquad (2.38)$$

$$K_{ij}=E_b I_b\int_0^L \phi_i^{(2)}(x)\phi_j^{(2)}(x)dx+E_p I_p\int_{x_1}^{x_2}\phi_i^{(2)}(x)\phi_j^{(2)}(x)dx \qquad (2.39)$$

$$P=E_p d_{31} a b_p\left[\left(\phi_1'(x_2)-\phi_1'(x_1)\right)\ \cdots\ \left(\phi_n'(x_2)-\phi_n'(x_1)\right)\right]^T \qquad (2.40)$$

$$L=\left[\phi_1(x_d)\ \cdots\ \phi_n(x_d)\right]^T \qquad (2.41)$$

$$q=\left[q_1\ \cdots\ q_n\right]^T \qquad (2.42)$$

The equation of motion can be expressed as:

$$M\ddot{q}(t)+Kq(t)=-PV_a+Lf_d(t) \qquad (2.43)$$

Further, the structural damping is included via Rayleigh damping:

$$C=\alpha M+\beta K \qquad (2.44)$$

where α and β can be determined from experiments.

If a state vector x is defined as:

$$x = [q_1 \quad \cdots \quad q_n \quad \dot{q}_1 \quad \cdots \quad \dot{q}_n]^T \tag{2.45}$$

The equation of motion can be expressed in the form of state equation:

$$\dot{x} = Fx + G_c V_a + G_d f_d \tag{2.46}$$

where

$$F = \begin{bmatrix} 0_{n\times n} & I_n \\ -M^{-1}K & -M^{-1}C \end{bmatrix} \tag{2.47}$$

$$G_c = -\begin{bmatrix} 0_{n\times n} & M^{-1} \end{bmatrix}^T P \tag{2.48}$$

$$G_d = \begin{bmatrix} 0_{n\times n} & M^{-1} \end{bmatrix}^T L \tag{2.49}$$

2.4 Sensing Model of the Piezoelectric Sensor

From structural mechanics, the stress T_1 at the mid plane of the bending piezoelectric element and its radius of curvature R are related by [15]:

$$T_1 = \frac{aE_p}{R} \tag{2.50}$$

where a is the distance from the mid plane of the piezoelectric element to the beam's neutral axis, as shown in Figure 2.3

For small deflections, the radius of curvature can be approximated as:

$$\frac{1}{R} = \frac{\partial^2 w}{\partial x^2} \tag{2.51}$$

Hence, the stress can be expressed as: $T_1 = aE_p \dfrac{\partial^2 w}{\partial x^2}$

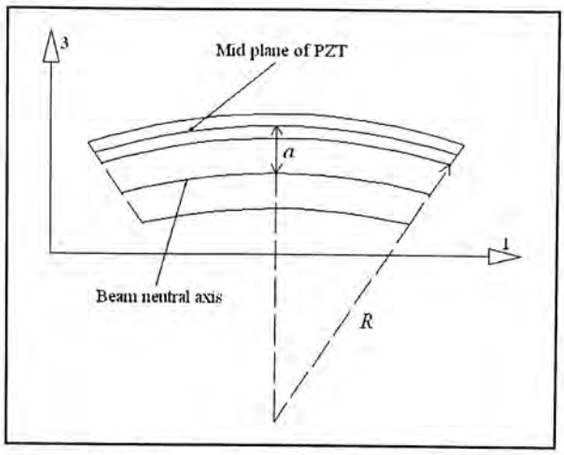

Figure 2.3 Side view of beam under bending

From the constitutive equation (2.5), the electrical charge generated due to mechanical deformation on the piezoelectric element per unit area is:

$$D_3 = d_{31} a E_p \frac{\partial^2 w}{\partial x^2}$$

Therefore, the total charge Q deposited on the piezoelectric element is:

$$Q = \int_A D_3 dA = \int_{x_1}^{x_2} E_p d_{31} a b_p \frac{\partial^2 w}{\partial x^2} dx$$

$$= E_p d_{31} a b_p \left[w'(x_2,t) - w'(x_1,t) \right] \qquad (2.52)$$

2.4.1 Strain Sensing Model

Once the piezoelectric element is charged, it can be considered as a parallel plate capacitor. We adopt an electrical equivalent model proposed by Dosch et al. [5] as shown in Figure 2.4. Let C_p be the equivalent capacitance of the piezoelectric element and V_p be the voltage source induced from the mechanical deformation. Thus using (2.52), the voltage induced across the piezoelectric element is found to be:

$$V_p = \frac{Q}{C_p} = \frac{E_p d_{31} a b_p}{C_p} \left[w'(x_2,t) - w'(x_1,t) \right] \qquad (2.53)$$

Since the approximate transverse displacement of the structure takes the form:

$$w(x,t) = \sum_{i=1}^{n} \phi_i(x) q_i(t)$$

$$w'(x_2,t)-w'(x_1,t)=\sum_{i=1}^{n}\phi_i'(x_2)q_i(t)-\sum_{i=1}^{n}\phi_i'(x_1)q_i(t)$$

$$=\sum_{i=1}^{n}\left[\phi_i'(x_2)-\phi_i'(x_1)\right]q_i(t)$$

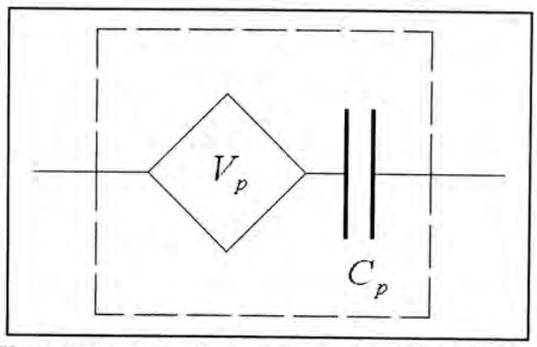

Figure 2.4 Electrical equivalent model of a piezoelectric element

Hence,

$$V_p=\frac{E_p d_{31} a b_p}{C_p}\sum_{i=1}^{n}\left[\phi_i'(x_2)-\phi_i'(x_1)\right]q_i(t)=\frac{1}{C_p}Jx \tag{2.54}$$

where x is defined as in (2.45) and

$$J=\left[P^T \quad 0_{1\times n}\right] \tag{2.55}$$

From the structure of matrix J, the induced voltage is proportional to the generalized coordinate q, so the measurement of V_p is equivalent to the strain sensing. The strain sensing can be realized by using the circuit as shown in Figure 2.5 in which V_c is an external (control) voltage applied to the structure and the output is defined as V_1. Using Kirchhoff law, the output is found to be:

$$V_1=\frac{C_p}{C_p+C_1}\left(V_c+V_p\right)$$

$$=\frac{C_p}{C_p+C_1}V_c+\frac{1}{C_p+C_1}Jx \tag{2.56}$$

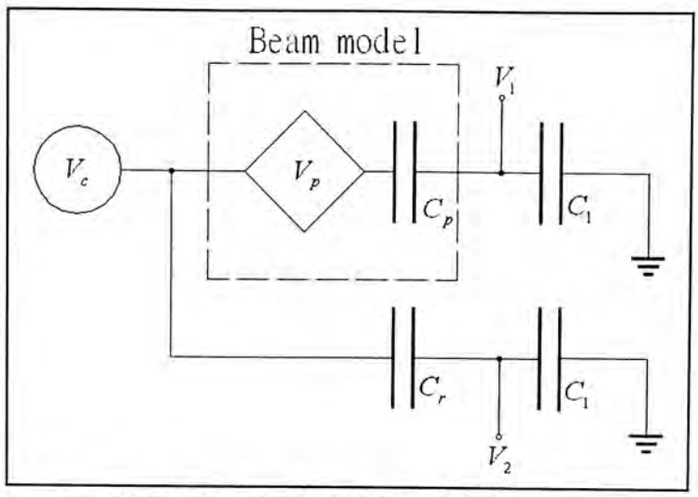

Figure 2.5 Strain sensing circuit

The effective voltage applied across the piezoelectric element is:

$$V_a = V_c - V_1 = \frac{C_1}{C_p + C_1} V_c - \frac{1}{C_p + C_1} Jx \tag{2.57}$$

Therefore, substituting (2.57) into (2.46), the overall dynamics of the composite beam with the self-sensing actuator is:

$$\dot{x} = \left(F - \frac{1}{C_p + C_1} G_c J \right) x + \left[\frac{C_1}{C_p + C_1} G_c \quad G_d \right] \begin{bmatrix} V_c \\ f_d \end{bmatrix} \tag{2.58}$$

2.4.2 Strain Rate Sensing Model

From (2.52), $Q = E_p d_{31} a b_p \left[w'(t, x_2) - w'(t, x_1) \right]$

The current induced by the piezoelectric element is:

$$I_p = \frac{dQ}{dt} = E_p d_{31} a b_p \left[\dot{w}'(t, x_2) - \dot{w}'(t, x_1) \right]$$

$$= E_p d_{31} a b_p \sum_{i=1}^{n} \left[\phi_i'(x_2) - \phi_i'(x_1) \right] \dot{q}_i(t) = \bar{J} \dot{x} \tag{2.59}$$

where

$$\bar{J} = \left[0_{1 \times n} \quad P^T \right] \tag{2.60}$$

From the structure of $\bar{J}$, the induced current is proportional to the rate of change of the generalized coordinate $\dot{q}$. Hence, the measurement of induced current I_p is equivalent to strain rate sensing. The strain rate sensing is achieved by using the circuit as shown in Figure 2.6. Similarly, V_c is the control voltage and the output is defined as V_1. Using Kirchhoff law, the output is:

$$V_1 = R_1 I_p + \left(\frac{R_1}{Z_{CR}}\right) V_c \tag{2.61}$$

where $Z_{CR} = \dfrac{1 + C_p R_1 s}{C_p s}$ is the resultant impedance of the series $C_p R_1$ configuration and s is the Laplace variable.

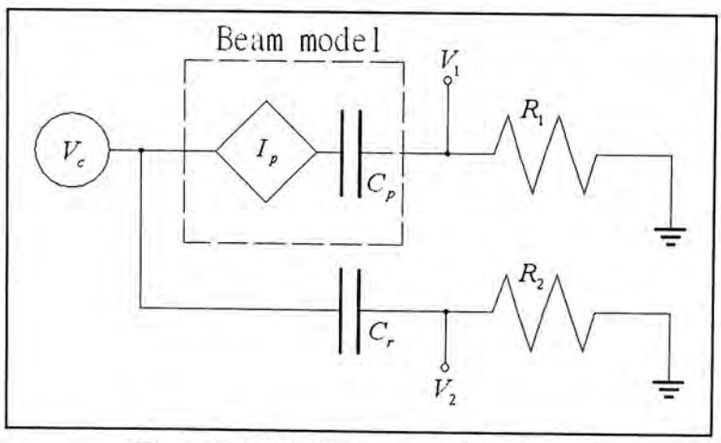

Figure 2.6 Strain rate sensing circuit

Since $V_1 = R_1 \bar{J} x + \dfrac{C_p R_1 s}{C_p R_1 s + 1} V_c$ (2.62)

Let $V_f = \dfrac{\eta}{s + \eta} V_c$ and $\eta = \dfrac{1}{C_p R_1}$

Then the output V_1 can be expressed as:

$$\dot{V}_f = -\eta V_f + \eta V_c \tag{2.63a}$$

$$V_1 = R_1 \bar{J} x + V_c - V_f \tag{2.63b}$$

Similar to the strain sensing circuit, the effective applied voltage is found to be:

$$V_a = V_c - V_1 = V_f - R_1 \bar{J} x \tag{2.64}$$

Therefore, substituting (2.63) and (2.64) into (2.46), the overall dynamics of the combined mechanical structure to the strain rate sensing circuit is:

$$\begin{bmatrix} \dot{x} \\ \dot{V}_f \end{bmatrix} = \begin{bmatrix} F - R_1 G_c \bar{J} & G_c \\ 0 & -\eta \end{bmatrix} \begin{bmatrix} x \\ V_f \end{bmatrix} + \begin{bmatrix} 0 & G_d \\ \eta & 0 \end{bmatrix} \begin{bmatrix} V_c \\ f_d \end{bmatrix} \tag{2.65}$$

In addition, for the frequency band of interest:

$$C_p R_1 s << 1 \tag{2.66}$$

such that the high pass RC circuit behaves close to a pure differentiator. The dynamics can be approximated as:

$$\dot{x} = \left(F - R_1 G_c \bar{J}\right) x + G_c V_c + G_d f_d \tag{2.67a}$$

$$V_1 = R_1 \bar{J} x + C_p R_1 s V_c = R_1 \bar{J} x + C_p R_1 \dot{V}_c \tag{2.67b}$$

2.5 Model Validation

The derived model of the composite structure is verified experimentally. In the experiment, there is no external voltage applied into the structure ($V_c = 0$). A hammer is used to hit near the fixed end of the beam. The tip displacement of the beam is recorded by a laser vibrometer (Polytec OFV-303). The applied force (input) and the measured displacement (output) were fed into a FFT analyzer (Ono-Sokki CF-3400) to generate the open loop frequency response of the structure. The parameters used in the simulation are listed in Table 2.1. The piezoelectric element used throughout this study is lead zirconium titanate (PZT). Both the simulation and experiment results are shown in Figure 2.7.

Table 2.1 System parameters

Number of modes modeled (n) 5	Location of disturbance acting (x_d) 8 [mm]	Beam Young's modulus (E_b) $7.5*10^{10}$ [N/m^2]	PZT Young's modulus (E_p) $6.2*10^{10}$ [N/m^2]
PZT constant (d_{31}) $-175*10^{-12}$ [m/V]	Beam length (L) 0.34 [m]	Beam density (ρ_b) 2700 [kg/m^3]	PZT density (ρ_p) 7600 [kg/m^3]
Location of PZT bonded (x_1, x_2) (17, 89.5) [mm]		Beam width (b_b) 25 [mm]	PZT width (b_p) 23 [mm]
Rayleigh damping (α, β) $(0.62, 0.9*10^{-6})$		Beam thickness (t_b) 3 [mm]	PZT thickness (t_p) 0.528 [mm]

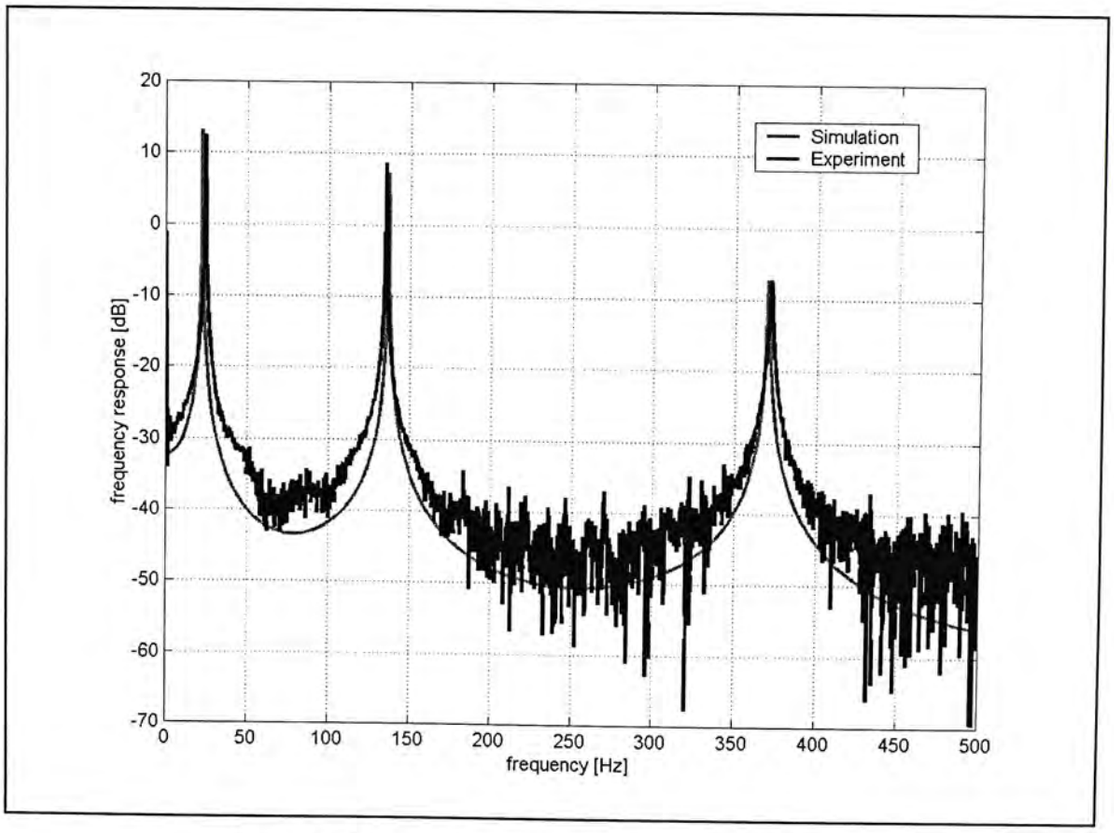

Figure 2.7 Comparison of open loop response

The frequency response function of the derived model was compared with the actual structural response. It shows the model matches closely to the actual system. The results also indicate that the first resonant mode has the highest peak amplitude and the peak amplitudes decrease with increasing modes.

Chapter 3

Control of Smart Structures

This chapter will give an overview of some control techniques that are widely used in the self-sensing smart structures, including strain rate feedback control and positive position feedback control. The second part of this chapter will present an adaptive algorithm based on online estimation to compensate the time varying uncertainties of the piezoelectric structure.

3.1 Strain Rate Feedback Control

Generally, a vibrating structure can be modeled by a set of ordinary or partial differential equations. For a system described by PDE, some approximation techniques could be applied to convert it into an ODE system, for example, Rayleigh-Ritz method, assumed-modes method, and Galerkin method, etc. As a result, the dynamics of the structure is governed by a set of second order differential equations. In scalar case, the open loop of such a system can be written as:

$$m\ddot{x} + c\dot{x} + kx = b_c u + b_d \hat{d} \tag{3.1}$$

where m is mass, c is damping, k is stiffness, b_c and b_d are the control and disturbance input gains respectively.

If the rate of change of state $\dot{x}$ is measurable, the proportional control law

$$u = -g\dot{x} \tag{3.2}$$

results in the following closed loop system:

$$m\ddot{x} + (c + b_c g)\dot{x} + kx = b_d \hat{d} \tag{3.3}$$

If g is chosen such that $b_c g$ is positive, the damping is increased. Further, The stability of the closed loop system is guaranteed by the condition:

$$c + b_c g > 0 \quad and \quad k > 0 \tag{3.4}$$

In the above discussion, only the structural dynamics is under consideration while those from sensors and actuators are neglected. As the control is generated based on the structural velocity, it is named as strain rate feedback control.

The strain rate feedback control can be extended to structure with multiple degree-of-freedom (DOF). Recalling the motion equation of the composite beam derived in chapter two:

$$\dot{x} = \left(F - R_1 G_c \bar{J}\right)x + G_c V_c + G_d f_d \tag{2.67a}$$

$$V_1 = R_1 \bar{J} x + C_p R_1 \dot{V}_c \tag{2.67b}$$

where the circuit is shown in Figure 2.6, the output V_1 is the sum of the signals due to the structural velocity and the rate of change of the control input. A bridge circuit is introduced to separate the control input from the circuit output. Define the bridge circuit output as:

$$V_s = V_1 - V_2 \tag{3.5}$$

Referring to Figure 2.6, if the time constants of both arms of the bridge circuit are equal, i.e., $C_p R_1 = C_r R_2$ (3.6)

$$V_s = R_1 \bar{J} x = R_1 \sum_{i=1}^{n} P_i \dot{q}_i \tag{3.7}$$

Here V_s is the sensing voltage that depends on the structural velocity only. Base on this sensing voltage, strain rate feedback control can be applied and the control input is found to be:

$$V_c = -BV_s = -BR_1 \bar{J} x = -BR_1 \sum_{i=1}^{n} P_i \dot{q}_i \tag{3.8}$$

where B is a positive scalar feedback gain. The closed loop dynamics becomes:

$$\dot{x} = \left(F - R_1 G_c \bar{J}\right)x - G_c B R_1 \bar{J}x + G_d f_d$$

$$\Rightarrow \dot{x} = \left(F - (1+B)R_1 G_c \bar{J}\right)x + G_d f_d \tag{3.9}$$

Obviously, the feedback gain can affect the pole location of the closed loop system. As long as the feedback gain is chosen such that all the eigenvalues of the matrix $F - (1+B)R_1 G_c \bar{J}$ have negative real part, the closed loop system is asymptotically stable.

The simple configuration of the strain rate feedback controller has the advantage of easy implementation, which makes it popular in self-sensing applications. The effectiveness of the strain rate feedback control will be demonstrated in the following simulations.

Using the smart beam model derived in chapter two, an impulse disturbance near the free end is input to actuate the beam. The strain rate feedback controller (3.8) is applied to suppress the beam vibration. The bridge circuit and controller parameters are listed in Table 3.1. The open loop beam tip displacement is shown in Figure 3.1a while the sensing voltage is shown in Figure 3.1b.

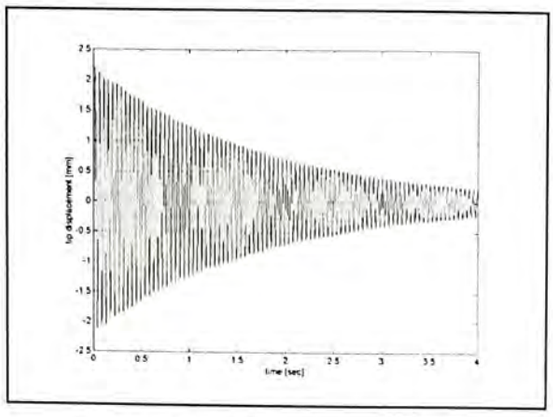

Figure 3.1a Open loop tip displacement

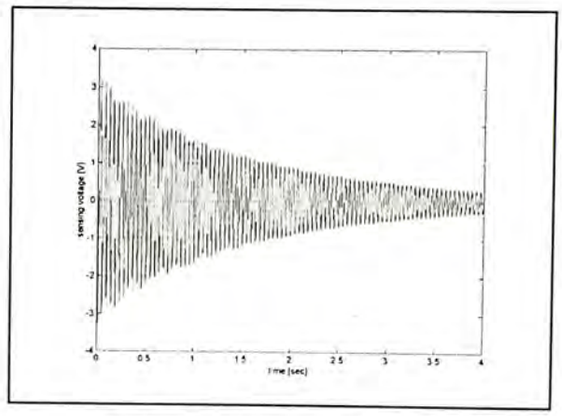

Figure 3.1b Open loop sensing voltage

The closed loop tip displacement is shown in Figure 3.2a. It shows that there is a significant reduction in settling time. The 10% settling time is decreased from 3.9 to

1.2 sec. The sensing and actuating voltage are shown in Figure 3.2b and 3.2c respectively. The control voltage magnitude is less than 30V and the closed loop eigenvalues are -1002.8 ± 7418.1i, -431.6 ± 4643.9i, -19.5 ± 2325.8i, -2.0 ± 138.9i, and -8.0 ± 859.3i.

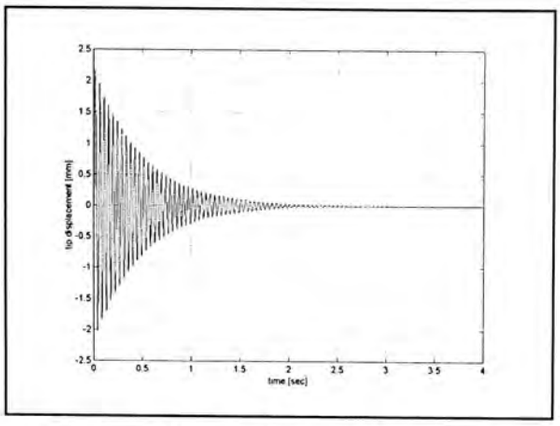

Figure 3.2a Closed loop tip displacement

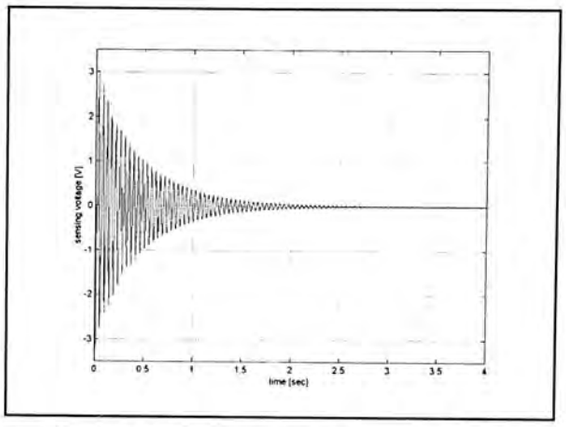

Figure 3.2b Closed loop sensing voltage

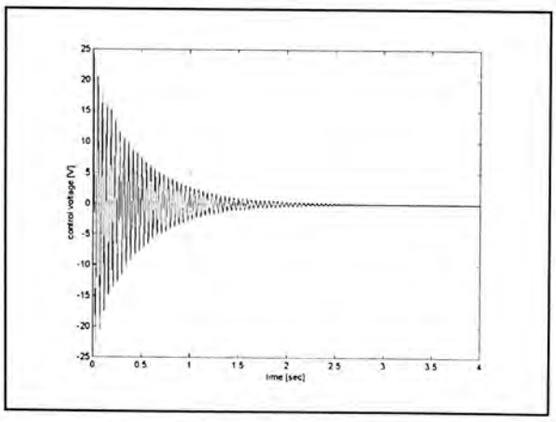

Figure 3.2c Control voltage

Table 3.1 Bridge circuit and strain rate feedback controller parameters

C_p	52 nF
C_r	52 nF
R_1	10 kΩ
R_2	10 kΩ
B	7.5

The strain rate feedback control can be considered as a special case of state feedback control. In the standard state feedback control, when the full state is measurable, the feedback gains can be individually assigned for each mode. On the other hand, strain rate feedback control directly amplifies the measured output by one feedback gain, i.e. unifying the feedback gains for all modes. In view of implementation, it is undesirable. Since the controller will also amplify the high frequency measurement noise. If the feedback gain is too large, the amplified noise will excite the high frequency dynamics of the structure. In addition, the strain rate sensing is based on

the high pass RC circuit. Noise amplification also decreases the signal to noise ratio of the sensing signal. To solve the high frequency gain problem, a low pass filter can be used to attenuate the high frequency signal from the sensor. This allows a higher feedback gain to be implemented to result in a better performance without exciting the high frequency dynamics. But this limits the controller to function at low frequency band only. Further, in order to achieve self-sensing actuation using strain rate feedback control, the frequency band of interest has to satisfy (2.66). But only the first resonant frequency of the smart beam satisfies this constrain, the self-sensing technique using strain rate feedback control can only be applied to suppress the first vibration mode of the structure.

3.2 Positive Position Feedback Control

Recalling the scalar vibrating system:

$$m\ddot{x} + c\dot{x} + kx = b_c u + b_d \hat{d}$$

$$y = hx$$

where y is a measurable output.

When the structure is connected to an auxiliary system described by:

$$\ddot{x}_f + c_f \dot{x}_f + k_f x_f = k_f g y \tag{3.10a}$$

$$u = x_f \tag{3.10b}$$

where c_f, k_f and g are damping, stiffness and input gain of the auxiliary system.

The closed loop system becomes:

$$\begin{bmatrix} \ddot{x} \\ \ddot{x}_f \end{bmatrix} + \begin{bmatrix} \frac{c}{m} & 0 \\ 0 & c_f \end{bmatrix} \begin{bmatrix} \dot{x} \\ \dot{x}_f \end{bmatrix} + \begin{bmatrix} \frac{k}{m} & -\frac{b_c}{m} \\ -k_f g h & k_f \end{bmatrix} \begin{bmatrix} x \\ x_f \end{bmatrix} = \begin{bmatrix} \frac{b_d}{m} \hat{d} \\ 0 \end{bmatrix} \tag{3.11}$$

It is asymptotically stable if and only if all the eigenvalues of the matrix:

$$\begin{bmatrix} 0 & 0 & 1 & 0 \\ 0 & 0 & 0 & 1 \\ -k/m & b_c/m & -c/m & 0 \\ k_f gh & -k_f & 0 & -c_f \end{bmatrix} \text{ have negative real part} \tag{3.12}$$

By choosing a positive damping coefficient and spring constant of the auxiliary system, the controller gain can be determined according to (3.12). As the controller (auxiliary system) uses the measured position signal to generate the control and feed back to the structure positively, it is named as positive position feedback control.

When the smart beam structure is integrated with the self-sensing circuit as shown in Figure 2.5, in term of state variable, the motion equation takes the form:

$$\dot{x} = \left(F - \frac{1}{C_p + C_1} G_c J \right) x + \begin{bmatrix} \frac{C_1}{C_p + C_1} G_c & G_d \end{bmatrix} \begin{bmatrix} V_c \\ f_d \end{bmatrix} \tag{2.58}$$

Using the following substitutions:

$$P = [P_1 \quad \cdots \quad P_n]^T \tag{3.13}$$

$$L = [L_1 \quad \cdots \quad L_n]^T \tag{3.14}$$

The equivalent motion equation, in term of generalized coordinate, can be expressed as:

$$\ddot{q} + M^{-1} C \dot{q} + M^{-1} \left(K - \frac{PP^T}{C_p + C_1} \right) q = -\frac{C_1}{C_p + C_1} M^{-1} P V_c + M^{-1} L f_d \tag{3.15a}$$

$$V_1 = \frac{P^T}{C_p + C_1} q + \frac{C_p}{C_p + C_1} V_c \tag{3.15b}$$

Similar to the strain rate configuration, the output of the strain sensing contains a direct transmission from the control input. A bridge circuit is used to cancel the influence of the control from the output. When the reference capacitance in the bridge circuit is equal to the equivalent capacitance of the PZT patch,

$$C_r = C_p \tag{3.16}$$

and the output of the bridge circuit is defined as: $V_s = V_1 - V_2$, hence,

$$V_s = \frac{1}{C_p + C_1} Jx = \frac{P^T}{C_p + C_1} q \tag{3.17}$$

Therefore, the sensing output is only proportional to the strain of the structure.

A positive position feedback controller described by:

$$\ddot{x}_c + D_C \dot{x}_c + K_c x_c = K_c G V_s \tag{3.18a}$$

$$V_c = I_{(1xnc)} x_c \tag{3.18b}$$

is used to suppress the vibration of the structure. Where nc is the number of structural modes to be suppressed, which is smaller than or equal to the number of modeled structural modes. $I_{(1xnc)}$ denotes a unity row vector of nc column and G is a $n_c \times 1$ gain vector. The damping and stiffness matrices of the controller are chosen to be diagonal with positive elements. Hence, the closed loop system becomes:

$$\begin{bmatrix} \ddot{q} \\ \ddot{x}_c \end{bmatrix} + \begin{bmatrix} M^{-1}C & 0 \\ 0 & D_C \end{bmatrix} \begin{bmatrix} \dot{q} \\ \dot{x}_c \end{bmatrix} +$$

$$\begin{bmatrix} M^{-1}\left(K - \dfrac{PP^T}{C_p + C_1}\right) & \dfrac{C_1 M^{-1} P I_{(1xnc)}}{C_p + C_1} \\ -\dfrac{K_c G P^T}{C_p + C_1} & K_c \end{bmatrix} \begin{bmatrix} q \\ x_c \end{bmatrix} = \begin{bmatrix} M^{-1} L f_d \\ 0 \end{bmatrix} \tag{3.19}$$

Since the structural mass and stiffness matrices can be diagonalized by modal transformation, the combined damping matrix can be considered as diagonal with positive elements (positive definite). Hence, the stability of the closed loop system depends on the controller gain vector G and controller stiffness matrix K_c.

The performance of the positive position feedback controller (PPF) is verified by simulation. The smart beam is modeled up to the first five vibration modes and a PPF

controller is designed to suppress the first three modes of vibration. The bridge and controller parameters are listed in Table 3.2.

The open loop responses of the tip displacement and sensing voltage are shown in Figure 3.3a and 3.3b. When comparing to the open loop strain rate sensing, the tip displacement of strain sensing decays slower. It can be explained by the energy-dissipating element of the strain rate sensing circuit. Since the resistor dissipates part of the induced electric energy, it provides an additional damping effect on the overall structure.

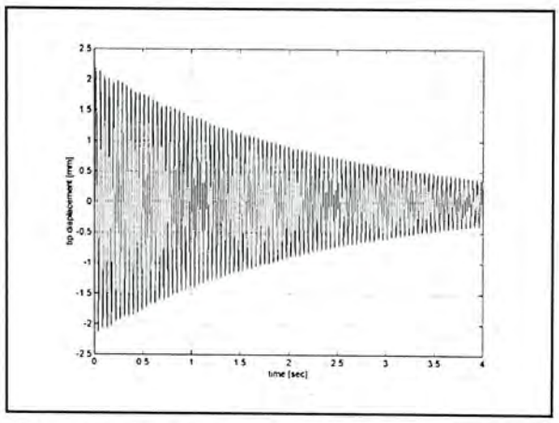

Figure 3.3a Open loop tip displacement

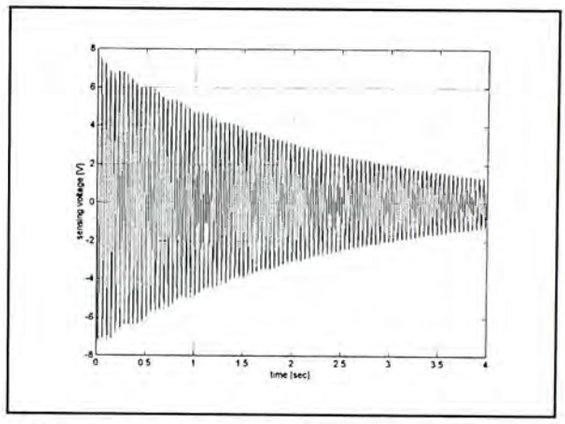

Figure 3.3b Open loop sensing voltage

The closed loop performances are shown in Figure 3.4. The 10% settling time of the vibration amplitude decreases from 6.5 to 1.2 sec. The maximum control voltage is about 80V, which is lager than that of the strain rate feedback controller.

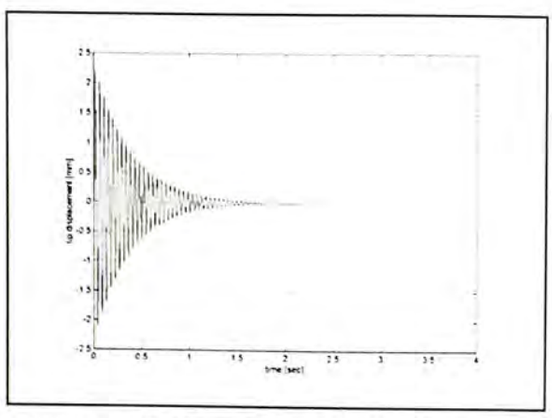

Figure 3.4a Closed loop tip displacement

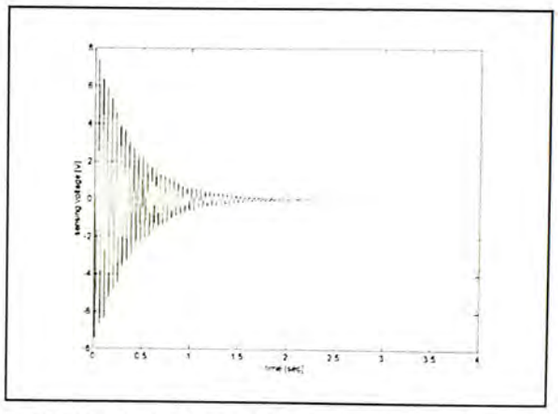

Figure 3.4b Closed loop sensing voltage

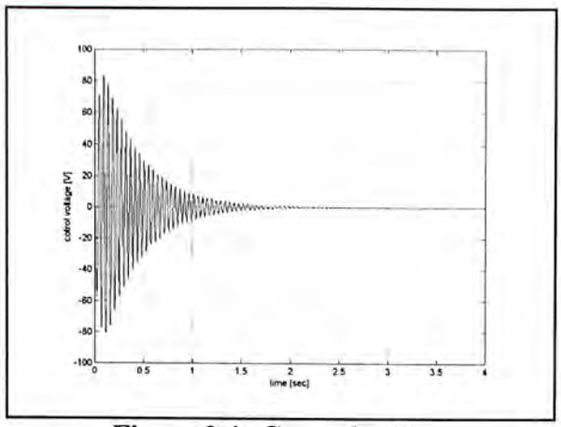

Figure 3.4c Control voltage

Table 3.2 Bridge circuit and PPF controller parameters

C_p	52 nF
C_r	52 nF
C_1	52 nF
D_c	*diag* (45.9, 670, 1809)
K_c	*diag* (153^2, 1117^2, 3016^2)
G	$[3 \quad 3 \quad 2]^T$

In view of filtering property, positive position feedback controller can be regarded as a set of low pass filters connected in parallel. Unlike strain rate feedback control, the roll off property of PPF has the advantage of guaranteed performance without exciting the high frequency dynamics. Therefore, PPF control can be applied to suppress higher vibration modes. The PPF controller design is based on the structural resonant frequencies and can be carried out without knowing the structural damping. In contrast to state feedback design in which both structural stiffness and damping have to be precisely known, the PPF controller offers a more flexible design. However, it is lacking of systematic method to design PPF controller parameters. Although some optimization techniques had been proposed to yield maximum closed loop damping, those approaches attempt to tune a single PPF controller only. In the above simulation, the controller damping ratios are chosen from 0.01 to 0.3 and the natural frequencies are 1 to 1.3 times greater than the corresponding structural natural frequencies.

3.3 Unbalanced Bridge Effect on Closed Loop Stability

To successfully implement self-sensing actuation using strain rate or positive position feedback control, the bridge circuit has to satisfy the balancing condition (3.6) (or (3.16)). In either case, this can be achieved if the equivalent capacitance of the PZT patch is exactly known. Since it has been reported [23] that the PZT capacitance varies with the ambience, using a fixed reference capacitor in the bridge circuit could not completely remove the direct transmission of control from the sensing output. In this section, the problem of an unbalanced bridge to the closed loop stability will be formulated.

Consider the strain rate sensing circuit with an unbalanced bridge and let

$$\sigma_r = C_p R_1 - C_r R_2 \neq 0 \tag{3.20}$$

Since the outputs of the two arms are:

$$V_1 = R_1 \bar{J} x + C_p R_1 \dot{V}_c \quad \text{and} \quad V_2 = C_r R_2 \dot{V}_c$$

the bridge output is: $V_s = V_1 - V_2 = R_1 \bar{J} x + \sigma_r \dot{V}_c$ (3.21)

Using strain rate feedback, the control voltage is found to be:

$$V_c = -BV_s = -BR_1 \bar{J} x - \sigma_r B \dot{V}_c \tag{3.22}$$

The closed loop system becomes:

$$\begin{bmatrix} \dot{x} \\ \dot{V}_c \end{bmatrix} = \begin{bmatrix} F - R_1 G_c \bar{J} & G_c \\ -\dfrac{R_1 \bar{J}}{\sigma_r} & -\dfrac{1}{\sigma_r B} \end{bmatrix} \begin{bmatrix} x \\ V_c \end{bmatrix} + \begin{bmatrix} G_d f_f \\ 0 \end{bmatrix} \tag{3.23}$$

Since the feedback gain B is positive, the closed loop system is stable if and only if

$$\sigma_r \geq 0 \text{ and the eigenvalues of } \begin{bmatrix} F - R_1 G_c \bar{J} & G_c \\ -\dfrac{R_1 \bar{J}}{\sigma_r} & -\dfrac{1}{\sigma_r B} \end{bmatrix} \text{ have negative real part} \tag{3.24}$$

Obviously, the system becomes unstable when $\sigma_r < 0$. This instability only depends on the bridge parameters and it shows the system has poor robustness with respect to

the bridge balancing. Further, it is impractical to exactly cancel the control from the bridge output. When the bridge is exactly balanced, a tiny decrement of the PZT capacitance immediately destabilizes the closed loop system. In the implementation, it always uses a promising capacitor to ensure $\sigma_r \geq 0$.

Consider the unbalanced strain sensing circuit and let

$$\sigma_s = \frac{C_p}{C_p + C_1} - \frac{C_r}{C_r + C_1} \neq 0 \tag{3.25}$$

Hence, the output of the bridge circuit is:

$$V_s = V_1 - V_2 = \frac{P^T}{C_p + C_1} q + \sigma_s V_c \tag{3.26}$$

Similar to the unbalanced strain rate sensing, the sensor output is corrupted with the control. Positive position feedback is applied to yield the closed loop system as:

$$\begin{bmatrix} \ddot{q} \\ \ddot{x}_c \end{bmatrix} + \begin{bmatrix} M^{-1}C & 0 \\ 0 & D_C \end{bmatrix} \begin{bmatrix} \dot{q} \\ \dot{x}_c \end{bmatrix} + \begin{bmatrix} M^{-1}\left(K - \dfrac{PP^T}{C_p + C_1}\right) & \dfrac{C_1 M^{-1} PI_{(1xnc)}}{C_p + C_1} \\ -\dfrac{K_c G P^T}{C_p + C_1} & K_c\left(I - GI_{(1xnc)}\sigma_s\right) \end{bmatrix} \begin{bmatrix} q \\ x_c \end{bmatrix} = \begin{bmatrix} 0 \\ 0 \end{bmatrix} \tag{3.27}$$

The effect of the unbalanced bridge circuit appears in the lower right partition of the combined stiffness matrix. The system remains stable as long as all the closed loop eigenvalues have negative real part. The overall stability depends on the controller parameters, K_c and gain vector G, as well as the bridge parameter C_r. Specifically, consider the scalar system of the controller dynamics:

$$\ddot{x}_c + D_C \dot{x}_c + K_c(1 - G\sigma_s)x_c = \frac{K_c G P}{C_p + C_1} q \tag{3.28}$$

When q is bound (assuming bound disturbance), the controller states are bound if and only if

$$D_c > 0 \qquad \text{and} \qquad \sigma_s < G^{-1} \tag{3.29}$$

It shows a tradeoff between the controller gain to the mismatch parameters. A high gain decreases the system robustness to the unbalanced bridge. This stability constraint differs from that of the strain rate sensing in the sense that complete cancellation of control is practical and the system remains stable for a little variation of the PZT capacitance.

The characteristics of the strain rate feedback and PPF control are summarized in Table 3.3.

Table 3.3 Comparison of strain rate feedback and PPF control

	Advantages	Disadvantages
Stain Rate Feedback	• Easy implementation • Additional damping effect from RC circuit	• Application limited to low frequency band • Highly sensitive to unbalanced bridge
Positive Position Feedback	• Wider frequency band application • Inherent robustness to unbalanced bridge	• Lack of systematic method to determine controller parameters.

3.4 Self-Compensation of Capacitance Variation

Since the bridge-balancing problem is critical to self-sensing actuation, an adaptive scheme is proposed to compensate for the capacitance uncertainty. As shown in last section that the strain rate sensing has high sensitivity to unbalanced bridge and the limitation on the frequency band of application, in order to suppress higher structural vibration modes, the adaptation scheme is combined with the positive position feedback controller which uses compensated strain signal. The adaptive mechanism is driven by an online estimator in which signals from a modified bridge circuit are used to identify the balancing condition.

Consider the circuit shown in Figure 3.5 and let

$$\theta = \frac{C_p}{C_p + C_1} \tag{3.31}$$

Instead of choosing a reference capacitor to balance the bridge, an adaptable gain is introduced and replaces the second arm of the bridge circuit. Let $\hat{\theta}$ be an estimate of θ.

When there is no mechanical vibration, i.e. $V_p = 0$,

$$V_1 = \frac{C_p}{C_p + C_1} w = \theta w \quad \text{and} \quad V_2 = \hat{\theta} w \tag{3.32}$$

Hence, the bridge is balanced when

$$V_1 - V_2 = \theta w - \hat{\theta} w = 0 \tag{3.33}$$

When the bridge loses balance, define the estimation error as:

$$e = V_1 - V_2 \tag{3.34}$$

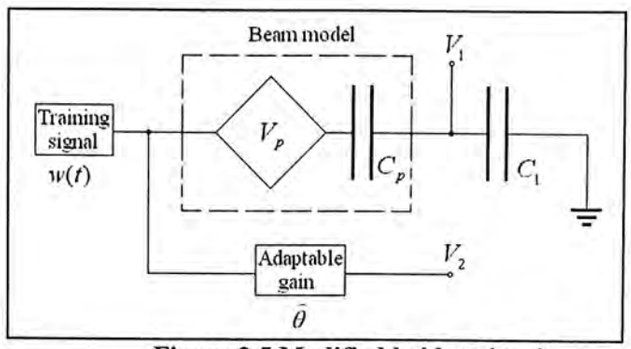

Figure 3.5 Modified bridge circuit

Therefore, the bridge-balancing problem is equivalent to design a gain adaptation to drive the estimation error to zero.

Define a cost function as:

$$S(\hat{\theta}) = \int_0^t e^{-\alpha(t-\tau)}\left[V_1(\tau) - w(\tau)\hat{\theta}\right]^2 d\tau \tag{3.35}$$

The cost function $S(\hat{\theta})$ can be considered as a weighted sum of the estimation error of the past data. The parameter α determines the weight of the data at a specific time instant. In order to increase the estimation accuracy during the capacitance variation, the most recent data are assigned the highest weight to reflect the importance of the current estimation error. On the other hand, those old data are assigned a lower weight and thus being forgetting by the cost function. The forgetting property is motivated by the fact that those old data are generated by old parameters and thus they should be discounted. Therefore, this technique is very effective in dealing with the estimation of varying parameters.

The cost function is minimized with respect to the estimated parameter. Hence, differentiating both sides of (3.35) with respect to $\hat{\theta}$ and set the derivative to zero yields:

$$\frac{dS(\hat{\theta})}{d\hat{\theta}} = 0 \quad \Rightarrow \quad 2\int_0^t e^{-\alpha(t-\tau)}(V_1(\tau) - w(\tau)\hat{\theta})(-w(\tau))d\tau = 0$$

$$\Rightarrow \qquad \int_0 e^{\alpha\tau} V_1(\tau) w(\tau) d\tau = \hat{\theta}\left[\int_0 e^{\alpha\tau} \left(w(\tau)\right)^2 d\tau\right] \tag{3.36}$$

Since the minimization has the effect of fitting all past data, it also has the advantage of averaging out the measurement noise over time.

Taking time derivative on both sides of (3.36) yields:

$$e^{\alpha t} V_1(t) w(t) = \dot{\hat{\theta}}\left[\int_0 e^{\alpha\tau} \left(w(\tau)\right)^2 d\tau\right] + \hat{\theta}\left[e^{\alpha t} \left(w(t)\right)^2\right]$$

$$\Rightarrow \qquad \dot{\hat{\theta}} = w(t) e(t) \left[\int_0 e^{-\alpha(t-\tau)} \left(w(\tau)\right)^2 d\tau\right]^{-1}$$

Define $$T(t) = \left[\int_0 e^{-\alpha(t-\tau)} \left(w(\tau)\right)^2 d\tau\right]^{-1} \tag{3.37}$$

Hence, the parameter update law is found to be:

$$\dot{\hat{\theta}} = w(t) e(t) T(t) \tag{3.38}$$

$T(t)$ has the physical meaning of amplifying the parameter adaptation and it is known as the adaptation gain. In order to achieve computational efficiency, instead of evaluating the adaptation gain by integrating (3.37) at every time instant, taking time derivative on both sides of (3.37) gives:

$$\dot{T}(t) = \left[\alpha e^{\alpha t} \int_0 e^{\alpha\tau} \left(w(\tau)\right)^2 d\tau - e^{\alpha t} e^{\alpha t} \left(w(t)\right)^2\right]\left[\int_0 e^{\alpha\tau} \left(w(\tau)\right)^2 d\tau\right]^{-2}$$

$$= \alpha\left[\int_0 e^{-\alpha(t-\tau)} \left(w(\tau)\right)^2 d\tau\right]^{-1} - \left(w(t)\right)^2 \left[\int_0 e^{-\alpha(t-\tau)} \left(w(\tau)\right)^2 d\tau\right]^{-2}$$

$$= \alpha T(t) - \left[w(t) T(t)\right]^2 \tag{3.39}$$

Hence, the adaptation gain $T(t)$ can be recursively computed using (3.39).

The dynamics of the estimator is governed by (3.38) and (3.39). To analyze the condition for parameter convergence, define the parameter error as:

$$\tilde{\theta} = \theta - \hat{\theta} \tag{3.40}$$

and consider the time derivative of the product $T^{-1}\tilde{\theta}$:

$$\frac{d}{dt}\left(T^{-1}\tilde{\theta}\right) = -T^{-2}\dot{T}\tilde{\theta} + T^{-1}(\dot{\theta} - \dot{\hat{\theta}})$$

$$= -T^{-2}\left\{\alpha T(t) - [w(t)T(t)]^2\right\}\tilde{\theta} - T^{-1}w(t)e(t)T(t)$$

$$= -\alpha T^{-1}\tilde{\theta}$$

Integration both sides yields:

$$\tilde{\theta}(t) = T(t)T^{-1}(0)\tilde{\theta}(0)e^{-\alpha} \tag{3.41}$$

In the above analysis, it is assumed that the rate of the parameter variation is negligible such that $\dot{\theta} \approx 0$. Hence, the parameter error $\tilde{\theta}$ converges to zero provided that the adaptation gain T is upper bounded. It shows that the training signal plays an important role in the estimation.

Besides the upper bounded condition on T, it should be noted that there is no disturbance acting and control applying in the above analysis ($V_p = V_c = 0$). The estimation is used to identify the open loop variation of θ only. For closed loop application, the bridge's first arm is no longer driven by training signal only. In addition, control signal and signal from structural deformation (result from disturbance) also appear at the first arm. Yet the self-compensation technique can be extended its application to closed loop system by using filters and choosing an appropriate training signal. For the vibration suppression problem, it assumes that the composite beam is generally subjected to low or mid frequency excitation (disturbance). Filter is designed based on the frequency band of application. Specifically, for the smart beam system, a pair of band pass filters is used to generate the signals for the estimator. The filters pass band is 1000-1100 Hz, which lies between the forth and fifth resonant modes of the beam structure. A low power band limited random signal is used as training signal. Hence, those low frequency signals,

the induced signal due to deformation and the control signal, will be filtered and left only the training signal input to the estimator. In implementation, the level of the random signal is chosen as low as possible but higher than the background measurement noise to obtain a satisfactory estimation.

The effectiveness of the estimator combined with a PPF controller for closed loop application will be verified through simulations. Figure 3.6 shows the detailed configuration of the combined design. The conventional bridge circuit is replaced by an estimator having the capability of self-balancing the bridge while concurrent control input is applied to suppress the beam vibration.

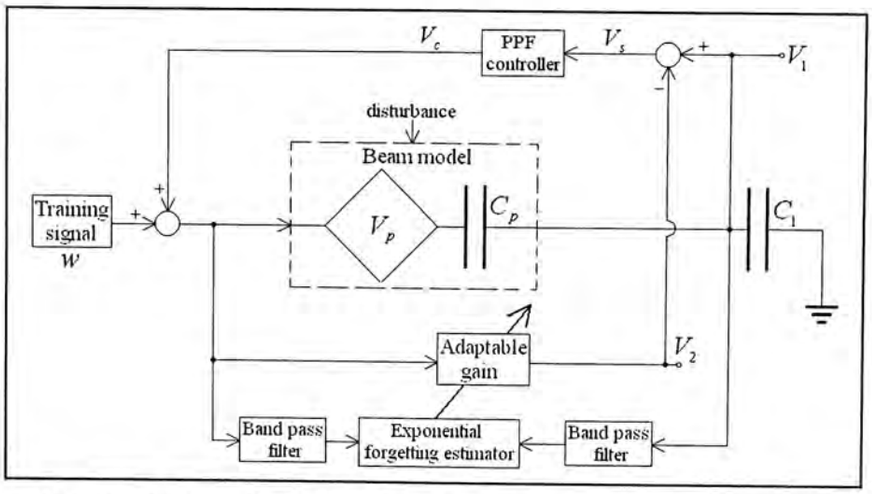

Figure 3.6 Combined adaptive design for closed loop application

In the simulation, the PZT capacitance is modeled as:

1. $C_p = C_{p_{nom}}(1+0.5\sin(0.05t))$

2. $C_p = C_{p_{nom}}(1+0.2e^{-0.1t})$

where $C_{p_{nom}}$ denotes the nominal value of PZT capacitance.

The parameters of the initial estimated gain, initial adaptation gain, forgetting factor and the value of C_1 are listed as follows:

Simulation 1

Initial gain: $\hat{\theta}(0) = 0.8$

Initial adaptation gain: $T(0) = 1000$

Forgetting factor: $\alpha = 2$

$C_1 = C_p(0) = 52\,\text{nF}$

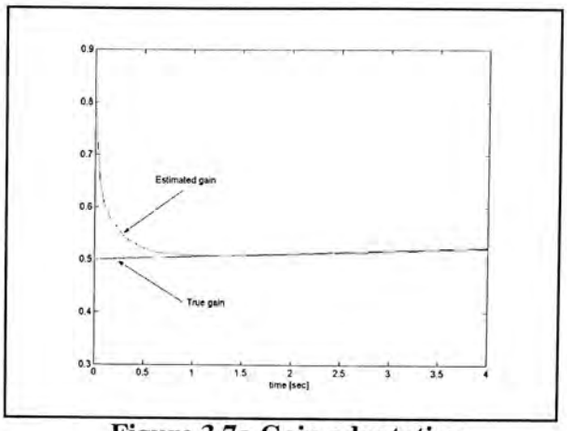

Figure 3.7a Gain adaptation

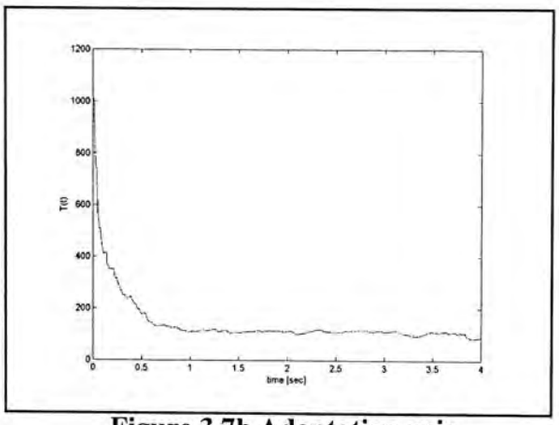

Figure 3.7b Adaptation gain

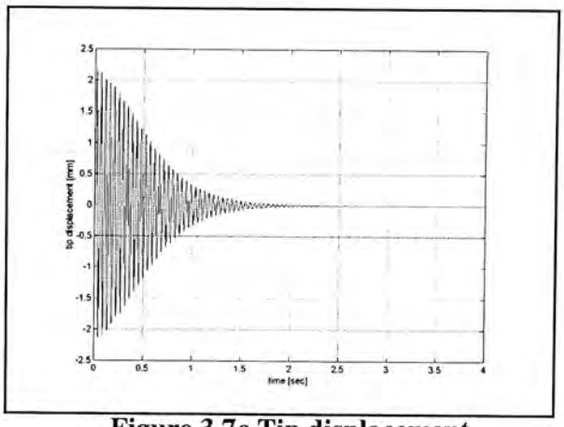

Figure 3.7c Tip displacement

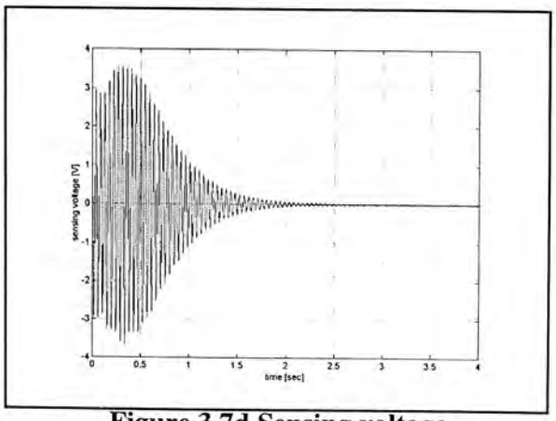

Figure 3.7d Sensing voltage

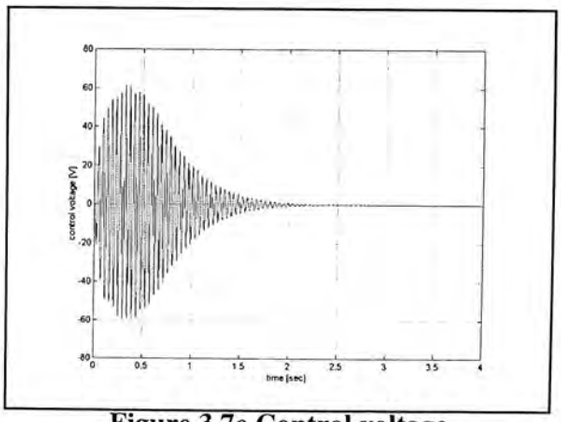

Figure 3.7e Control voltage

In the simulation, the beam is initially subjected to an impulse disturbance. Figure 3.6a shows that the estimated gain can track closely to the true gain variation. The sharp initial convergence is due to the selection of a high initial adaptation gain. Figure 3.7b shows the adaptation gain is upper bound and this guarantees the convergence of the estimated parameter to the true value. The performance of the

combined design is illustrated in Figure3.6c. It shows that the PPF controller can suppress the vibration during the parameter estimation.

Simulation 2

Initial gain: $\hat{\theta}(0) = 0.4$

Initial adaptation gain: $T(0) = 1000$

Forgetting factor: $\alpha = 2$

$C_1 = C_p(0) = 62.4\,\text{nF}$

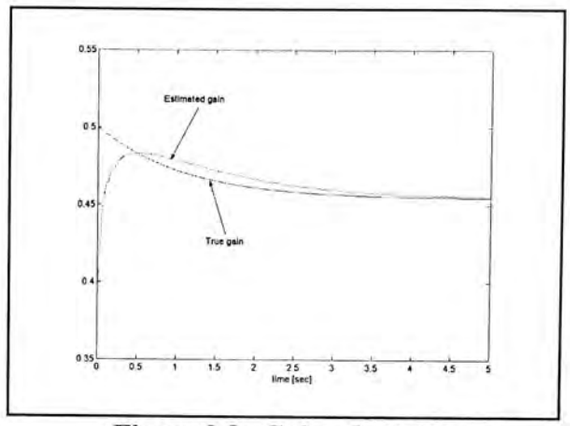

Figure 3.8a Gain adaptation

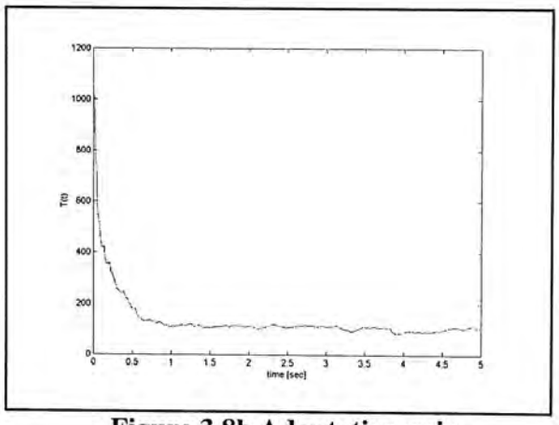

Figure 3.8b Adaptation gain

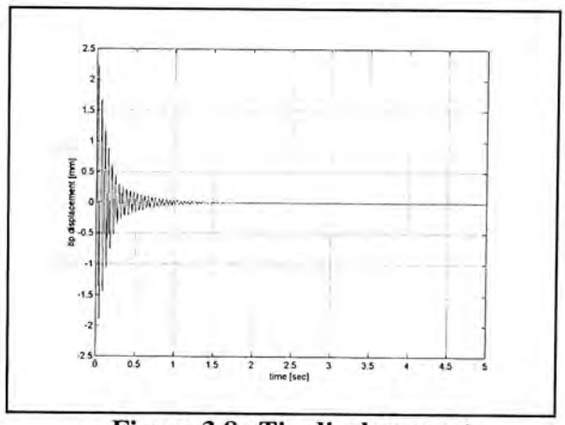

Figure 3.8c Tip displacement

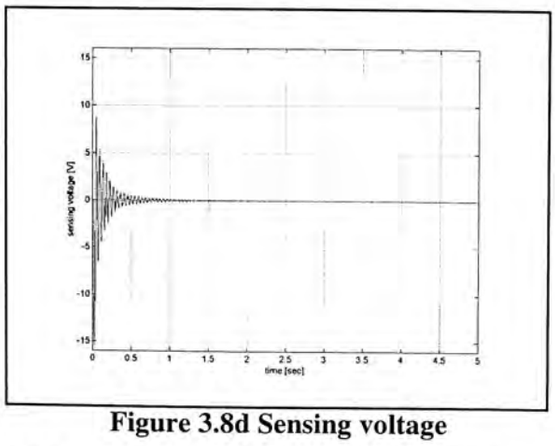

Figure 3.8d Sensing voltage

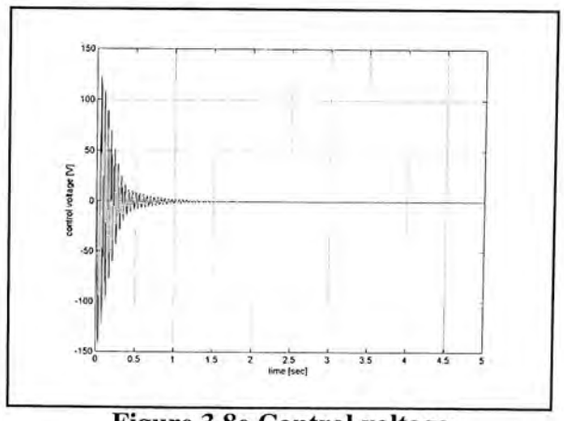

Figure 3.8e Control voltage

The second simulation results are shown in Figure 3.7. Basically, the convergence of the estimated gain is verified as the previous simulation. In this case, the high initial adaptation gain results an overshoot of the estimated parameter. But in the second simulation, the performance of the controller seemed to be better while the same controller is used in both simulations. This can be explained by the initial condition

of the bridge circuit. In the first case, $\tilde{\theta}(0) = \sigma_s < 0$. From (3.28), this is equivalent to increase the controller stiffness (or decreasing the effective gain of the controller). So the controller performance worse than the case of balanced bridge. On the other hand, for the second case, $\tilde{\theta}(0) = \sigma_s > 0$. The effective gain of the controller is increased provided that $K_c\left(I - GI_{(1xnc)}\sigma_s\right)$ is positive definite. Hence the controller appears to outperform the first case. It also indicates the implication of the bridge condition to the controller performance.

Chapter 4

Experimental Studies

In this chapter, the self-sensing control combined with adaptive compensation is implemented for the smart cantilever beam. The performance of the closed loop system will be evaluated under the conditions of changing bridge parameter and temperature. Also the performance of the system with and without adaptive compensation would be compared.

4.1 Experiment Setup

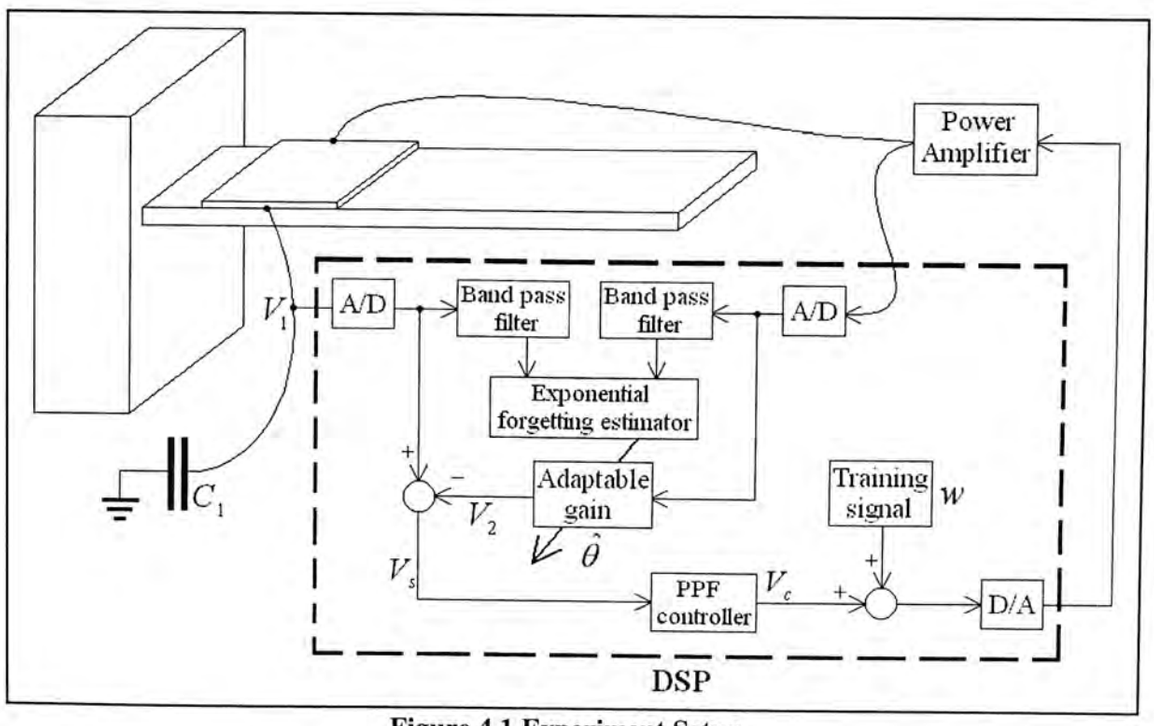

Figure 4.1 Experiment Setup

The complete configuration of the system is shown in Figure 4.1. The composite beam is connected to an external circuit. The circuit outputs a strain signal, which is due to the mechanical deformation of the structure, mixed with the control input. Both the control input and the signal from the external circuit are discretized by an

A/D converter and fed into a digital computer. The two signals are filtered and input to the estimator. Concurrently, the strain signal is extracted from the total response (V_1) using the estimated parameter ($\hat{\theta}$). The compensated strain signal is used to generate control input via the positive position feedback controller. The designed control input is summed with a low power training signal, which is used for parameter estimation, and converted into continuous time signal and then amplified by an external amplifier.

The bridge circuit, filters, estimator, training signal and control law implementations are all realized with a digital signal processor (DSP) as shown in the dashed box of Figure 4.1. They are programmed by Matlab / Simulink and downloaded into the DSP (dSPACE DSP 1102) through the supporting software. A band limited random signal is used as training signal. The A/D and D/A converters are sampled at 2.5 kHz. The filters are designed in discrete time domain while the controller are designed in continuous time domain and then discretized using Tustin's method:

$$s = \frac{2}{T}\left(\frac{1-z^{-1}}{1+z^{-1}}\right) \tag{4.1}$$

where T is the sampling period of the controller.

The discretized controller and all other digital components realized in the DSP are sampled with the same frequency of the A/D and D/A converters.

4.2 Experiment Results

4.2.1 Open Loop Response

A disturbance is input near the tip of the beam to excite the structure. A laser vibrometer is used to measure the tip displacement and the sensing voltage V_1 is recorded by computer. The results are presented in Figure 4.2a and 4.2b.

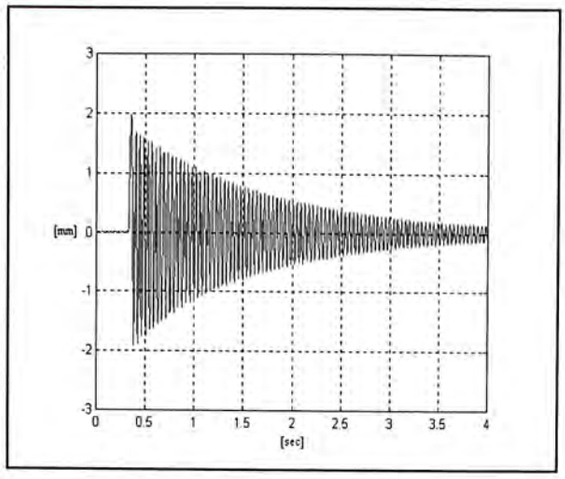

Figure 4.2a Open loop tip displacement

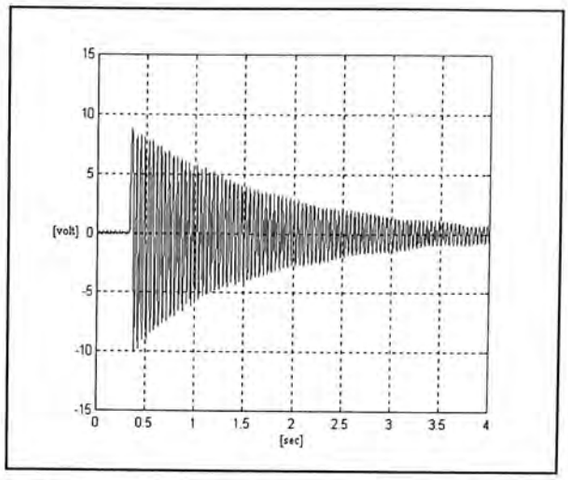

Figure 4.2b Open loop sensing voltage

4.2.2 Closed Loop Response with Balanced Bridge

In this experiment, positive position feedback control is applied to suppress the beam vibration. The PZT equivalent capacitance C_p has a nominal value 52nF at room temperature. The capacitor C_1 in the external circuit is chosen to have the same value such that the bridge can be balanced by a fixed gain: $\hat{\theta} = \dfrac{C_p}{C_p + C_1} = 0.5$

This configuration is equivalent to the conventional bridge circuit. The beam is excited by an impulse disturbance near the free end and the closed loop response is shown in Figure 4.3. The performance of the PPF controller can be recognized in the reduction of the settling time.

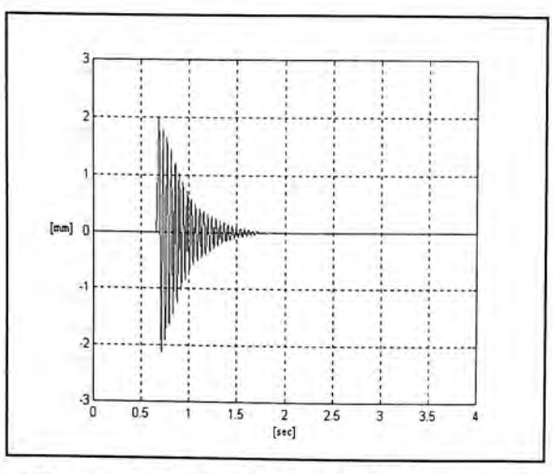

Figure 4.3a Closed loop tip displacement (balanced bridge with fixed gain)

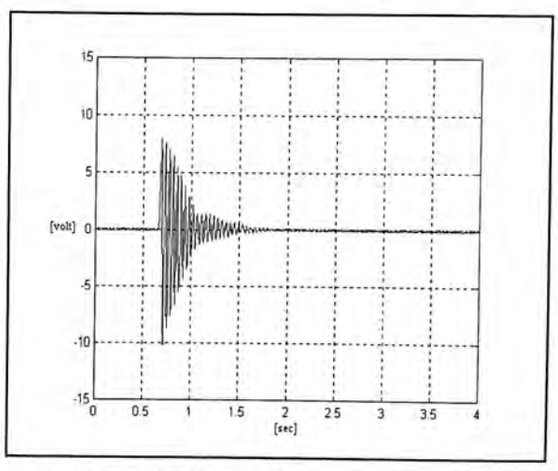

Figure 4.3b Closed loop sensing voltage (balanced bridge with fixed gain)

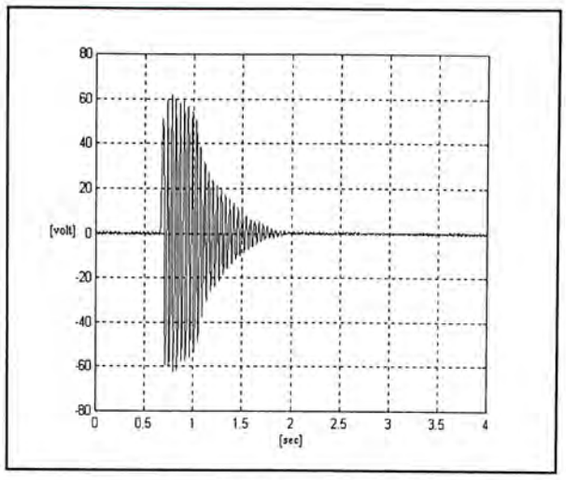

Figure 4.3c Closed loop control voltage
(balanced bridge with fixed gain)

The same experiment is conducted with the fixed gain replaced by the adaptive compensation. An initial gain value $\hat{\theta}(0) = 0.5$ is assigned to the estimator. The performance of the PPF controller combining the adaptive compensation is shown in Figure 4.4. Comparing to the previous experiment in which fixed gain is used, results show that there is slightly reduction in settling time from about 1 sec to 0.7 sec. It may be due to a tiny deviation of the real PZT capacitance from its nominal value and cause a slightly unbalanced effect.

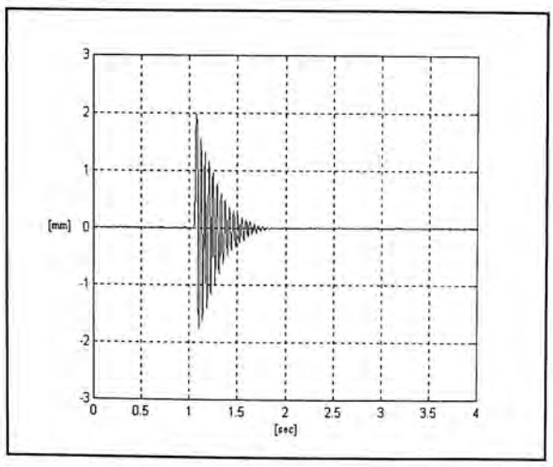

Figure 4.4a Closed loop tip displacement
(with self compensation)

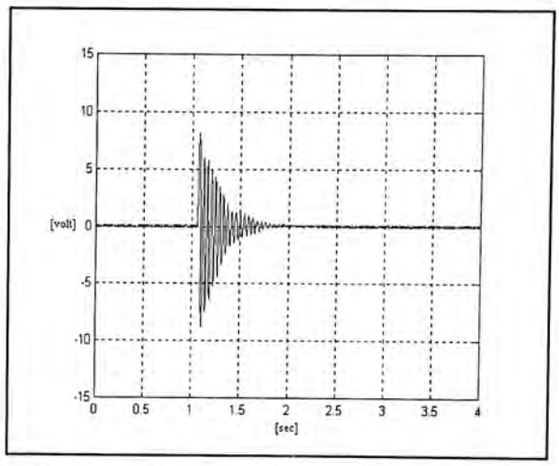

Figure 4.4b Closed loop sensing voltage
(with self compensation)

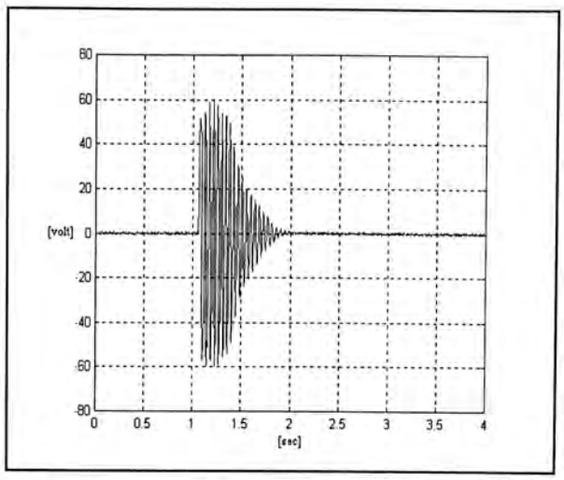

Figure 4.4c Closed loop control voltage
(with self compensation)

4.2.3 Closed Loop Response with Unbalanced Bridge

In this experiment, the capacitor C_1 is chosen to be 65nF while the fixed gain $\hat{\theta} = 0.5$ is kept unchanged so that the bridge is intended to be unbalanced. This is equivalent to a 20% decrement of the PZT capacitance. The performance of the closed loop system is shown in Figure 4.5. The vibration amplitude decays slower than the ideal case in which the bridge is balanced.

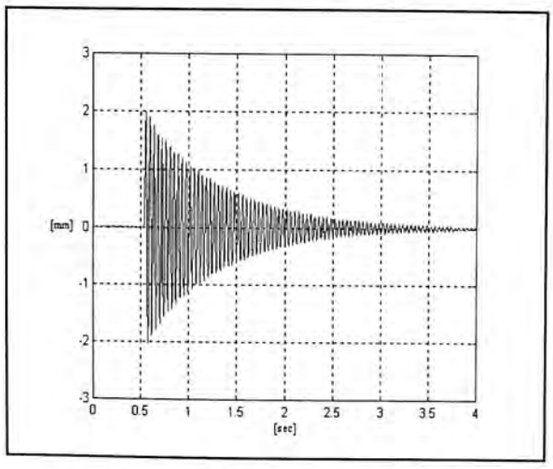

Figure 4.5a Closed loop tip displacement
(with unbalanced bridge)

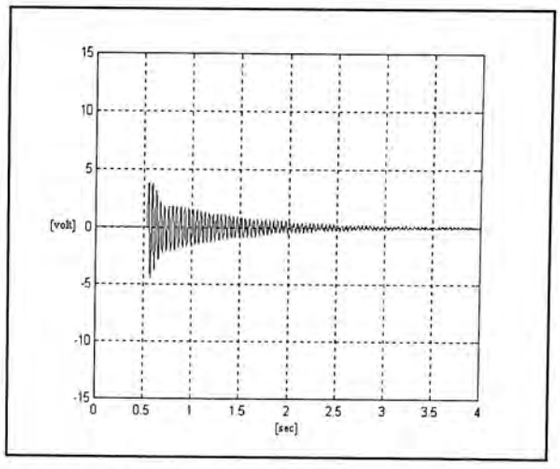

Figure 4.5b Closed loop sensing voltage
(with unbalanced bridge)

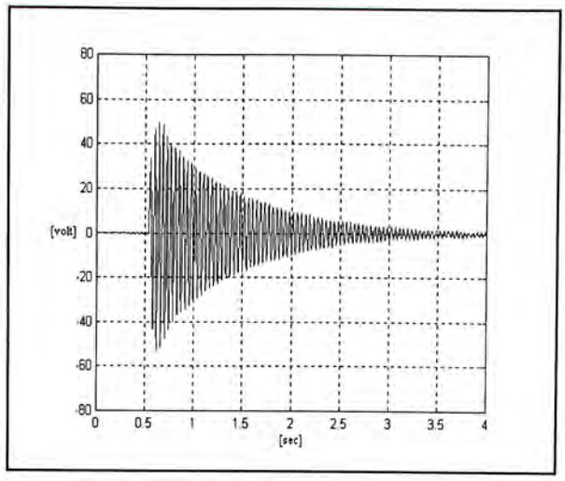

Figure 4.5c Closed loop control voltage
(with unbalanced bridge)

The results can be explained by the corrupted sensing signal. From the bridge parameter, $\sigma_s = -0.056$ (from (3.25)), hence the sensing signal is weakened by the control input. But it is worth noting that the closed loop system is still stable. This verifies both the degradation of performance and the inherent robustness of the strain sensing circuit with respect to slightly unbalanced bridge.

The same value of C_1 (65nF) is used and the adaptive compensation, with an initial gain $\hat{\theta}(0) = 0.5$, is applied instead of using a fixed gain. The results are shown in Figure 4.6. The effectiveness of the adaptive compensation is verified. From Figure 4.6a, the tip displacement decays much faster than the results in section *4.2.2* in which $C_1 = 52$nF.

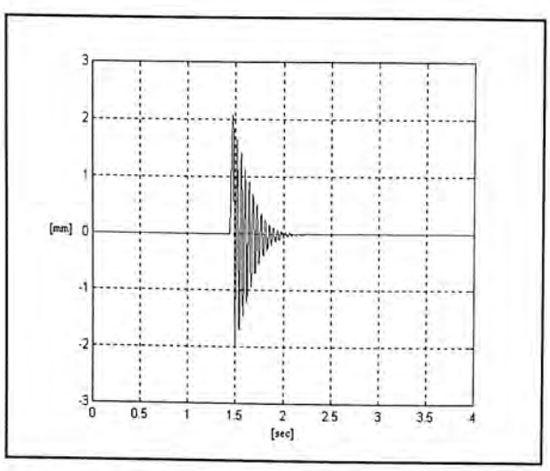

Figure 4.6a Closed loop tip displacement
(with self compensation)

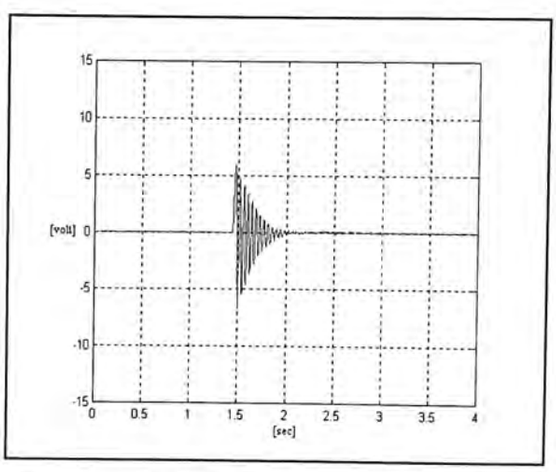

Figure 4.6b Closed loop sensing voltage
(with self compensation)

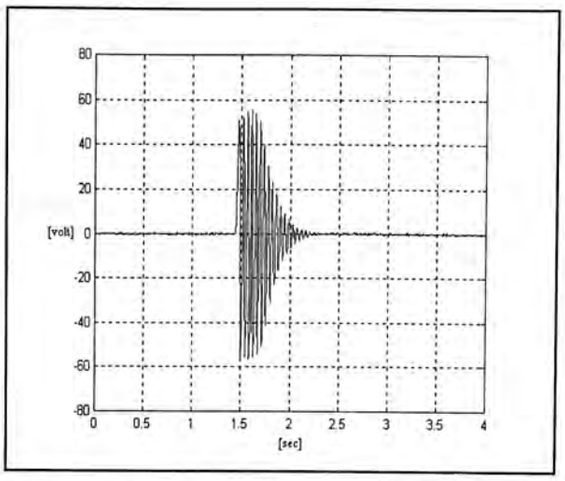

Figure 4.6c Closed loop control voltage (with self compensation)

The performance improvement is due to the increase of effective gain of the controller results from the increase of C_1. Hence the performance of the combined design is experimentally verified and the results show that the closed loop performance is guaranteed when the bridge is slightly unbalanced.

4.2.4 Closed Loop Response upon Sudden Change in Bridge Parameter

In this section, experiments were conducted by suddenly changing the bridge parameter of the closed loop system under the disturbance free condition ($V_p = 0$). Consider the circuit as shown in Figure 4.7, an additional capacitor C_a is used to change the equivalent parameter of the bridge by closing the switch.

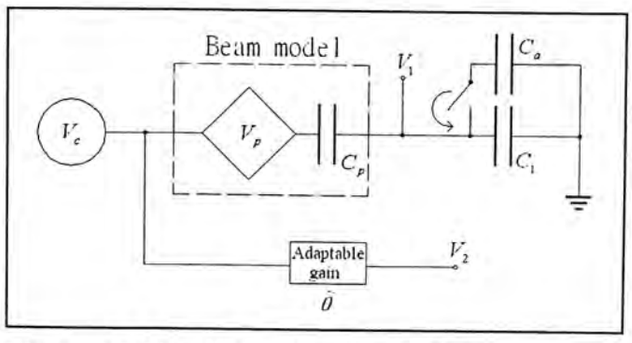

Figure 4.7 Circuit for changing bridge parameter

In the experiment, C_a = 25nF, C_1 = 52nF and the gain is fixed at 0.5. This configuration is equivalent to 35% decrement of the nominal PZT capacitance. The results of the sensing and control voltage are shown in Figure 4.8.

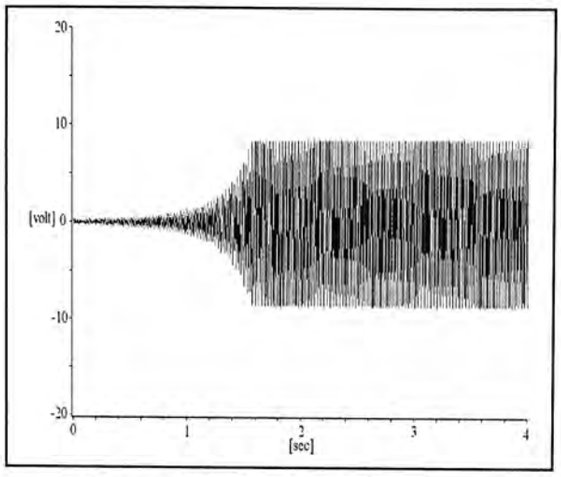

Figure 4.8a Sensing voltage

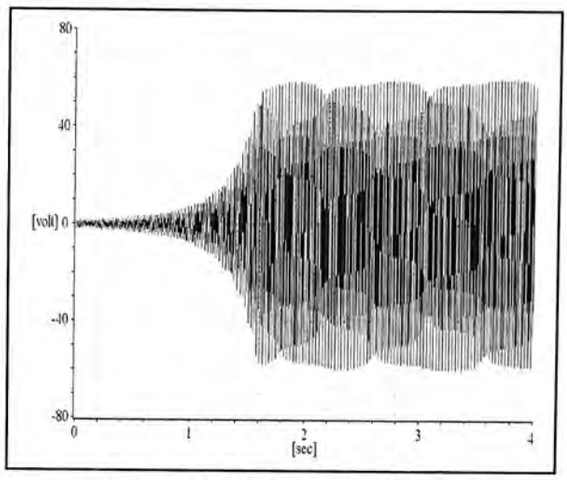

Figure 4.8b Control voltage

Since the system is disturbance free, initially both sensing and control voltages are nearly zero (but corrupted with measurement noise). When the switch is closed, the bridge is unbalanced and both signals gradually diverge.

The same experiment is conducted with the fixed gain replaced by the adaptive compensation. The results are shown in Figure 4.9. It appears that the sensing and control signals are kept near zero. In addition, the estimated gain is plotted versus time in Figure 4.9c. This shows the capability of the adaptive compensation to drive the estimated parameter to the true value after the switch is closed. It should be pointed out that the non-zero level of the sensing and control signals is the sum of the measurement noise and the training signal used by the estimator.

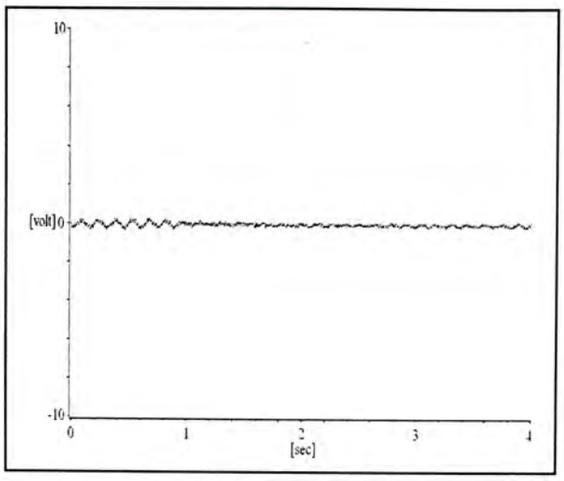

Figure 4.9a Sensing voltage

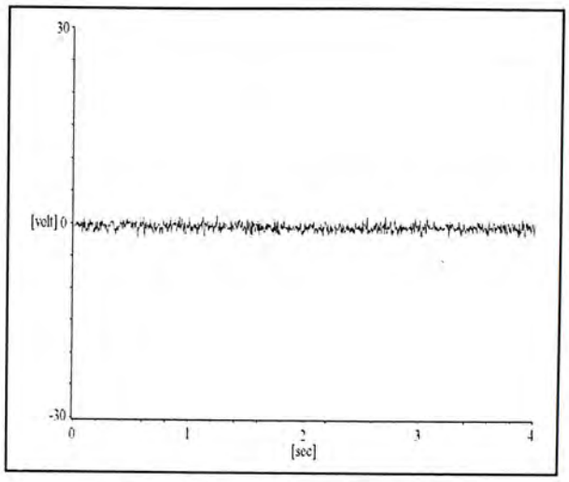

Figure 4.9b Control voltage

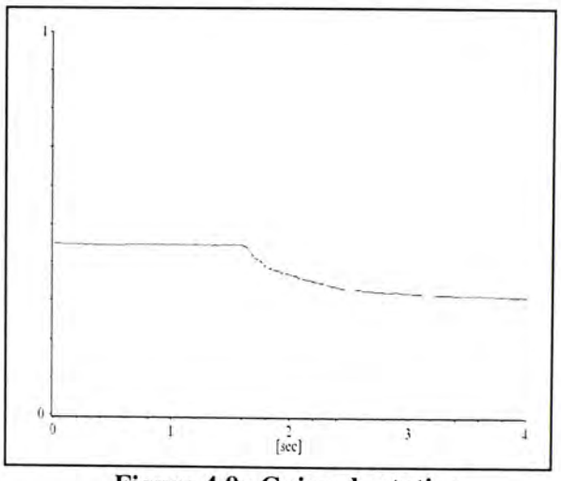

Figure 4.9c Gain adaptation

If the value of C_a is further increased to 50nF, which is equivalent to 49% change of the PZT capacitance, the results of using fixed gain and adaptive compensation are shown in Figure 4.10 and 4.11, respectively. For the case of fixed gain compensation, the sensing and control signals diverge rapidly after closing the switch. This experiment illustrates the result of violating the stability condition stated in (3.30). Theoretically, Both signals would be unbounded. However, the output saturation of the DSP and the op-amp of the interface circuit limit the magnitude of the control voltage. As shown in Figure 4.10b, the saturation is about 70V. Hence, the sensing and control signals appear fluctuation within the saturation limits.

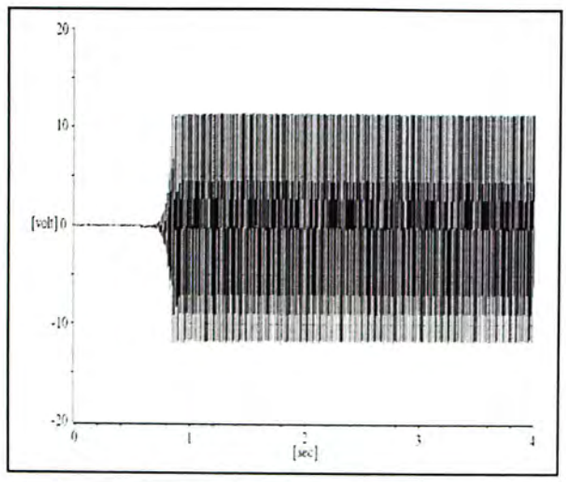

Figure 4.10a Sensing voltage

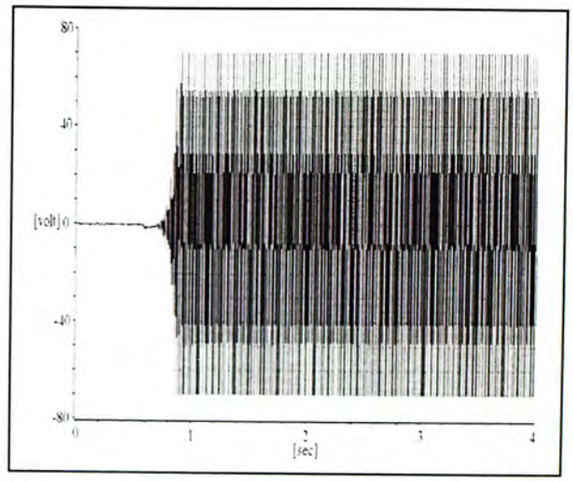

Figure 4.10b Control voltage

The result of adaptive compensation is presented in Figure 4.11. As shown in Figure 4.11a and 11b, there is a beat after the switch is closed. Simultaneously, from Figure 4.11c, the estimated gain converges to a new value to compensate for the parameter change.

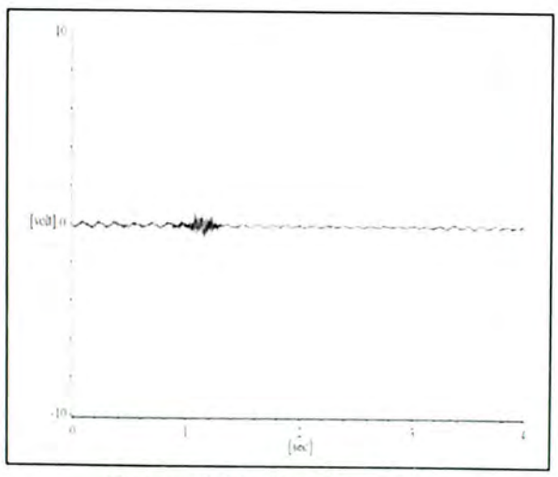

Figure 4.11a Sensing voltage

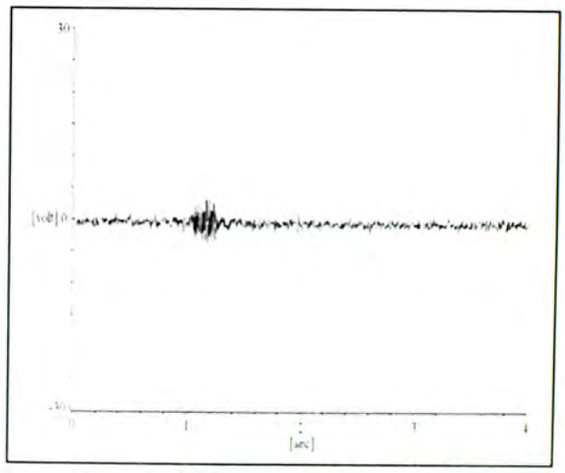

Figure 4.11b Control adaptation

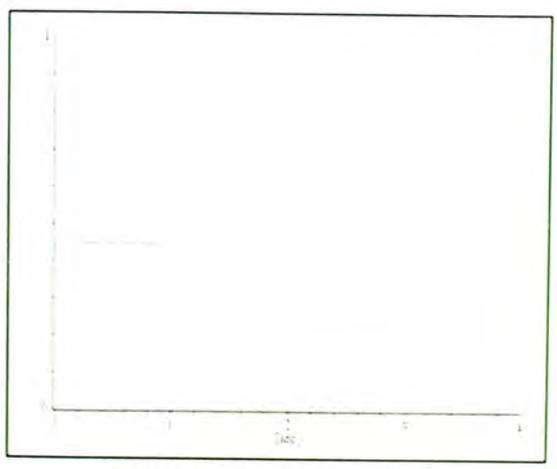

Figure 4.11c Gain adaptation

In last experiment, it appears unrealistic to consider about 50% change in PZT capacitance, yet it should be emphasized that the system is disturbance free. The closed loop system using fixed gain compensation would be more likely to become unstable with a smaller capacitance variation. Hence, it is worth testing the capability of the adaptive compensation upon such amount of uncertainty.

4.2.5 Closed Loop Response upon Temperature Variation

In this experiment, the adaptive scheme is tested under temperature variation. As it has been reported that the PZT capacitance is related to the ambient temperature, in contrast to those experiments conducted by changing the bridge parameter, this experiment provide a realistic variation of the actual PZT capacitance.

In the experiment, the adaptive scheme and the controller are set active. Concurrently, hot air was blown onto the PZT patch. The surface temperature of the PZT patch is recorded by a laser thermometer (MINOLTA). Figure 4.12a shows the steady state of the estimated gain, which is about 0.45. The capacitor C_1 is chosen to be 52nF. Hence the calculated value of PZT capacitance is 42.5nF. Figure 4.12b shows the surface temperature variation of the PZT patch when the hot air is being blown onto the patch.

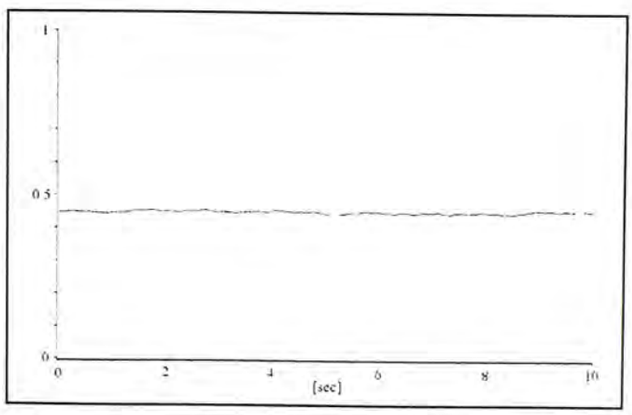

Figure 4.12a Steady state of the estimated gain

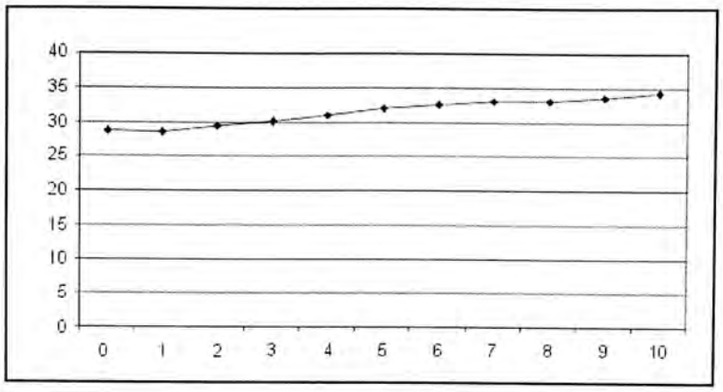

Figure 4.12b Temperature variation during heating

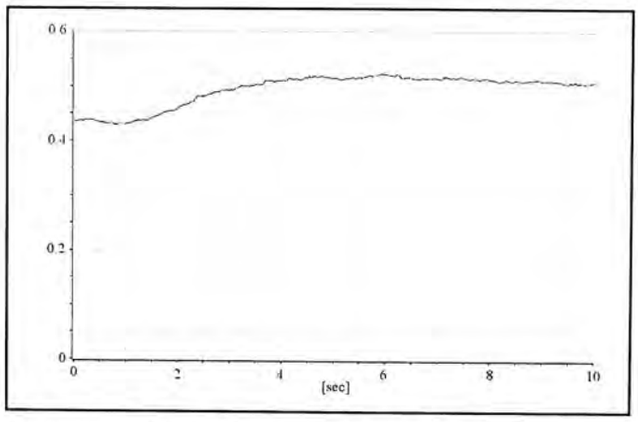

Figure 4.12c Gain adaptation during heating

The estimated gain during heating is shown in Figure 4.12c. It shows that the estimated gain gradually increases from its old steady state to a new value. It verifies that the adaptive scheme is responsive to the temperature variation. The new estimated value is about 0.51 and the percentage change of the PZT capacitance is about 27%.

4.2.6 Frequency Response

In this experiment, a hammer is used to hit near the fixed end of the beam to excite the vibration. The input force and the tip displacement are used to generate the frequency response. The closed loop and the open loop response of the system are compared. The first, second and third modes of the frequency response are shown in Figure 4.13a, b and c respectively. The results indicate that the PPF controller has the

highest vibration suppression capability at the first mode. The first mode peak magnitude approximately decreases 20dB.

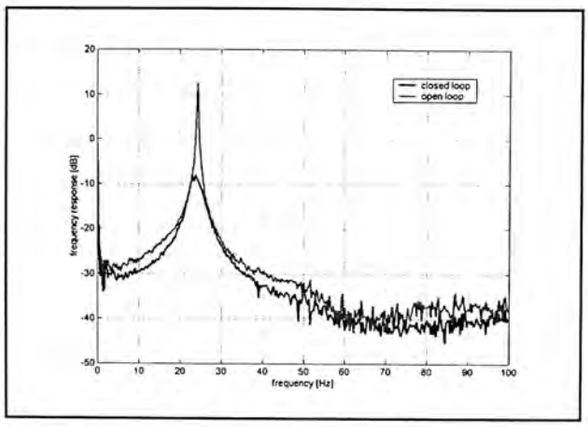

Figure 4.13a Frequency response – 1st mode

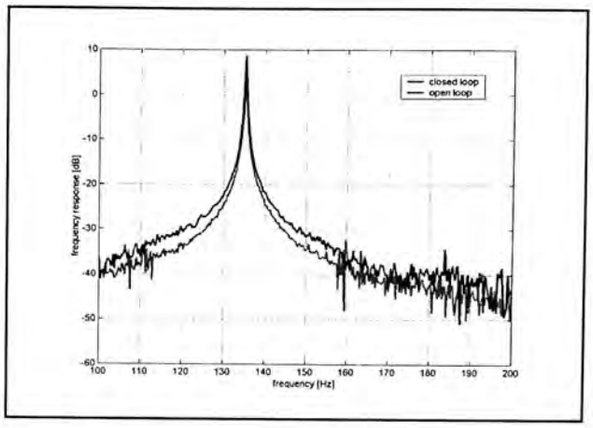

Figure 4.13b Frequency response – 2nd mode

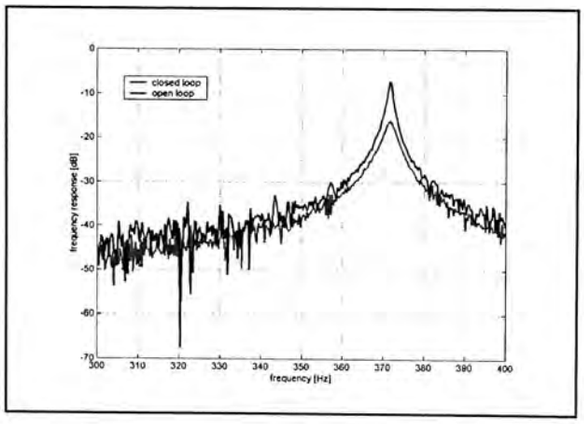

Figure 4.13c Frequency response – 3rd mode

The PPF controller has a relatively weaker vibration suppression effect at the second and third mode. The peak magnitude of second mode decreases about 6dB and the third mode decreases about 10dB. Since the damping effect of the controller depends on the location of the PZT bonded, as the PZT is bonded near the fixed end and the first mode has a relative larger strain there, the controller has a lager damping effect for the first mode and weaker for the others.

A simulation study on the open loop and closed loop frequency response is shown in Figure 4.14. It verifies that the controller has the highest vibration suppression

capability for the first mode. The damping ratios for both experiment and simulation closed loop and open loop systems are listed in Table 4.1.

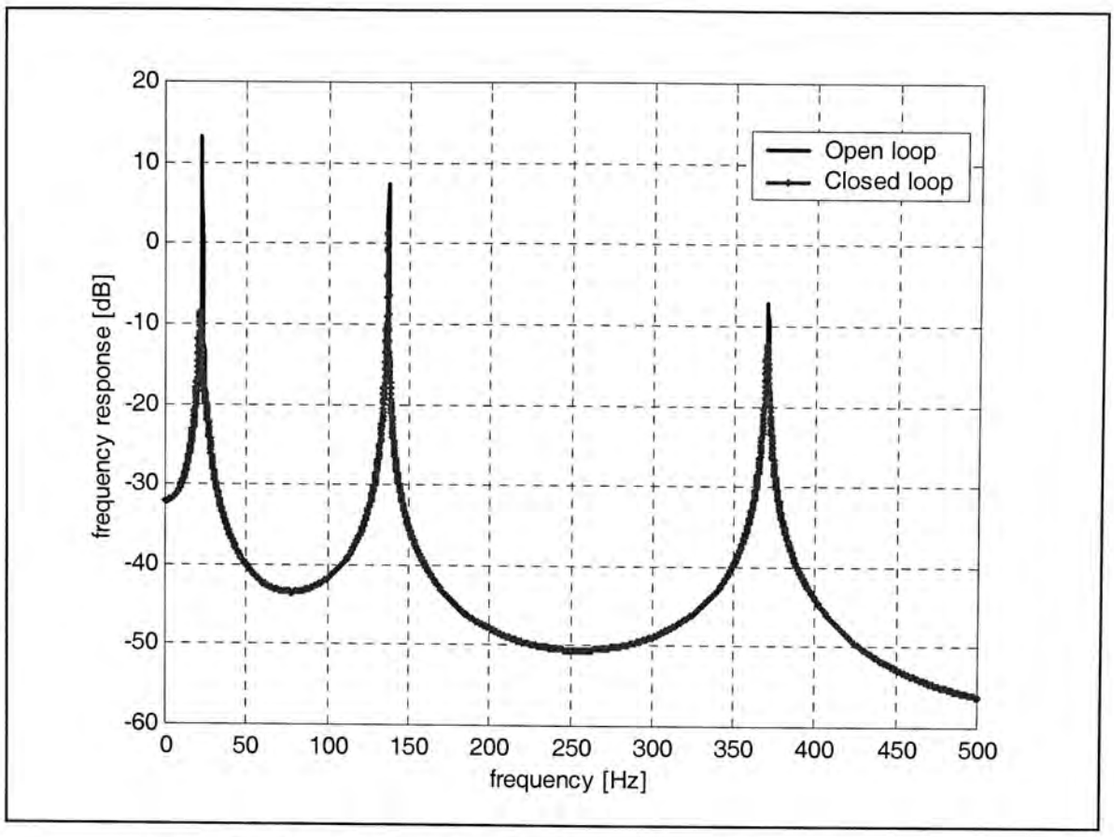

Figure 4.14 Simulation of open and closed loop frequency response

Table 4.1 Damping ratio of experiments and simulations

		First mode	Second mode	Third mode
Experiments	Open loop	0.59 %	0.11 %	0.16 %
	Closed loop	5.96 %	0.20 %	0.41 %
Simulations	Open loop	0.49 %	0.13 %	0.16 %
	Closed loop	4.88 %	0.18 %	0.29 %

Chapter 5

Summary

5.1 Conclusion

In this thesis, a study on the structural vibration control using self-sensing piezoelectric actuators is presented. The findings of this thesis are summarized as below:

- **Modeling.** The dynamic modeling of a smart beam structure with a surface bonded piezoelectric element undergoing transverse vibration is derived using Hamilton's principle. Owning to the continuous nature, its equation of motion is approximated to a standard state space representation using Galerkin's method. An external circuit for both senor and actuator functions is integrated to the piezo-based structure to yield an electromechanical system. The overall system is validated by experiments and the results show the derived model matches closely to the actual system. It should be noted that the mechanical properties of the structural system, the mass, damping and stiffness matrices, could be determined from a simpler frequency response approach. Particularly the Rayleigh damping is usually determined from experiment. However, as the present of the varying piezoelectric capacitance and the feed forward dynamics, it is insufficient to evaluate the structural input and output matrices using frequency approach.
- **Controller design.** Two controllers are designed using strain rate feedback and positive position feedback control. The effectiveness of both controllers

is verified through simulations. The effect of unbalanced bridge to close loop stability is formulated and it has been found that the strain sensing circuit has certain degree of robustness with respect to unbalanced bridge while the poor robustness of strain rate sensing has been proved. An adaptive compensation is proposed by combining the strain sensing circuit with the PPF controller for closed loop applications. The effectiveness of the combined design is verified through simulations and the results show the capability of concurrent self-compensation and vibration suppression.

- **Implementation.** The combined design is implemented to the smart beam structure via a digital signal processor. Several experiments are conducted to test the combined adaptive compensation for closed loop applications. Experiment results show that the adaptive design can self-tune the bridge circuit to maintain the balanced condition. The performances of the system by using fixed compensation and adaptive compensation are compared and it has been found that self-compensation keeps the high performance under an unbalanced bridge. Further, the self-compensation is tested under temperature variation and experiment results show the capability of the adaptive mechanism to respond under a realistic capacitance variation.

5.2 Future Work

Finally, some possible extensions of the current study are suggested in the following:

- Because of the fixed structural configuration, the designed controller is found to have higher vibration suppression capability for some particular modes than others. Thus it is worth analyzing the parameters such as size and location of the PZT bonded to optimize the controller performance. Further,

for complex structures like truss structures in which multiple self-sensing actuators are required, the current study could be extended to investigate the problem of controlling large complex structures using distributed self-sensing actuators and decentralized controllers.

- The passive vibration control of the piezo-based structure has been extensively studied recently. Also, as pointed out in this thesis, circuit elements would provide additional damping effect to the overall structure. Hence, in addition to actively suppress the vibration using the designed controller, a well-designed shunt circuit could be integrated, in which acts as an energy absorber to dissipate part of the energies, to yield an active-passive hybrid vibration controller.
- As hystersis nonlinearity of piezoelectricity become significant with large applied electric field, only low power application is considered in this thesis. In order to extend the current work to more high performance applications, further research on nonlinear piezoelectric models and nonlinear control methods should be explored.

Bibliography

[1] E.H. Anderson and N.W. Hagood, "Simultaneous Piezoelectric Sensing/ Actuation: Analysis and Application to Controlled Structures", Journal of Sound and Vibration 174(5), pp 617-639, 1994.

[2] E. Brusa, S. Carabelli, and A. Tonoli, "Modeling and Testing of Plate Structures Using Self-Sensing Piezoelectric Transducers", SPIE Conference on Smart Structures and Integrated Systems, Vol. 3329, pp 802-811, 1998.

[3] I. Bruant, G. Coffignal, F. Léné and M. Vergé, "Active Control of Beam Structures with Piezoelectric Actuators and Sensors: Modeling and Simulation", Journal of Smart Materials and Structures, vol. 10, pp 404-408, 2001.

[4] R.L. Clark, W.R. Saunders and G.P. Gibbs, "Adaptive Structures: Dynamics and Control", Wiley, 1998.

[5] J.J. Dosch, D.J. Inman and E. Garcia, "A Self-Sensing Piezoelectric Actuator for Collocated Control", Journal of Intelligent Material Systems and Structures, Vol. 3, pp 166-185, 1992.

[6] J.J. Dosch, D.J. Leo and D.J. Inman, "Comparison of Vibration Control Schemes for a Smart Antenna", Proceedings of the Conference on Decision and Control", pp 1815-1820, 1992.

[7] G.F. Franklin, J.D. Powell and A. Emami-Naeini, "Feedback Control of Dynamic Systems", Addison-Wesley, 3rd edition, 1994.

[8] M.I. Friswell and D.J. Inman, "The Relationship Between Positive Position Feedback and Output Feedback Controllers", Journal of Smart Materials and Structures", Vol. 8, pp 285-291, 1999.

[9] E. Garcia and L.D. Jones, "Self-Sensing Control Applied to Smart Material Systems", Structronic Systems: Smart Structures, Devices & Systems, Part 1, pp 37-60, 1998.

[10] S.F. Griffin, A.J. Bronowicki and R.S. Betros, "Piezoceramic Sensors and Actuators for Smart Composite Structures", Proceedings of the Conference on Decision and Control, pp 2543-2545, 1991.

[11] P. Horowitz and W. Hill, "The Art of Electronics", Cambridge University Press, 1989.

[12] L. Jones and E. Garcia, "Self-Sensing Magnetostrictive Actuator for Vibration Suppression", Journal of Guidance, Control, and Dynamics, vol. 19, pp 713-715, 1996.

[13] L. Jones, E. Garcia and H. Waites, "Self-Sensing Control as Applied to A PZT Stack Actuator Used as A Micropositioner", Journal of Smart Materials and Structures, Vol. 3, pp 147-156, 1994.

[14] B. Ko and B.H. Tongue, "Acoustic Control Using a Self-Sensing Actuator", Journal of Sound and Vibration 187(1), pp 145-165, 1995.

[15] B.B. Low, "Strength of Materials", Longmans, 2nd edition, 1995.

[16] J.A. Main, E. Garcia and D.V. Newton, "Precision Position Control of Piezoelectric Actuators Using Charge Feedback", Journal of Guidance, Control, and Dynamics, Vol. 18, pp 1068-1073, 1995.

[17] W.J. Manning, A.R. Plummer and M.C. Levesley, "Vibration Control of a Flexible Beam with Integrated Actuators and Sensors", Journal of Smart Materials and Structures, Vol. 9, pp 932-939, 2000.

[18] L. Meirovitch, "Fundamentals of Vibrations", McGraw-Hill, 2001.

[19] F. Pourboghrat and M. Daneshdoost, "Smart Actuators for Active Vibration Control", SPIE Conference on Smart Structures and Integrated Systems, Vol. 3329, pp 608-619, 1998.

[20] F. Pourboghrat and H. Pongpairoj, "Vibration Control of Flexible Structures Using Self-Sensing Actuators", Third International Symposium on Intelligent Automation and Control, pp 9918-9923, 2000.

[21] J. -J Slotine and W. Li, "Applied Nonlinear Control", Prentice Hall, 1991.

[22] T. Takigami, K. Oshima and Y. Hayakawa, "Application of Self-Sensing Actuator to Control of a Cantilever Beam", Proceedings of American Control Conference, pp 1867-1872, 1997.

[23] J. Tani, G.G. Cheng and J. Qiu, "Effectiveness and Limits of Self-Sensing Piezoelectric Actuators", Proceedings of International Workshop on Structural Health Monitoring, pp 502-514, 1997.

[24] J.S. Vipperman and R.L. Clark, "Implementation of An Adaptive Piezoelectric Sensoriactuator", AIAA Journal, Vol. 34, pp 2102-2109, 1996.

[25] S.Y. Wang, S.T. Quek and K.K. Ang, "Vibration Control of Smart Piezoelectric Composite Plates", Journal of Smart Materials and Structures, vol. 10, pp 637-644, 2001.

[26] S.M. Yang and C.A. Jeng, "Structural Vibration Suppression by Concurrent Piezoelectric Sensor and Actuator", Journal of Smart Materials and Structures, Vol. 5, pp 806-813, 1996.